ARTICLE

# *Cis,cis,trans*-[$Pt^{IV}Cl_2(NH_3)_2(perillato)_2$], a dual-action prodrug with excellent cytotoxic and antimetastatic activity

Received 00th January 20xx,
Accepted 00th January 20xx

DOI: 10.1039/x0xx00000x

Mauro Ravera,[a] Elisabetta Gabano,[a] Ilaria Zanellato,[a] Beatrice Rangone,[a] Elena Perin,[a] Beatrice Ferrari,[b] Maria Grazia Bottone [b] and Domenico Osella *[a]

Two Pt(IV) conjugates containing one or two molecules of perillic acid [(4-isopropenylcyclohexene-1-carboxylic acid], an active metabolite of limonene, were synthesized both with traditional and microwave-assisted methods and characterized. Their antiproliferative activity was tested on a panel of human tumor cell lines. In particular, *cis,cis,trans*-[$Pt^{IV}Cl_2(NH_3)_2(perillato)_2$] exhibited excellent antiproliferative and antimetastatic activity on A-549 lung tumor cells at nanomolar concentrations. A number of *in vitro* biological tests were performed to decipher some aspects of its mechanism of action, including transwell migration and invasion as well as wound healing assay.

## Introduction

The main obstacle to any effective chemotherapeutic treatment is the possible occurrence of tumor metastasis, that is the spread of cancer cells from the primary tumor to surrounding tissues and to distant organs. In fact, despite the success of the traditional therapeutic management of many cancers, that can control the growth of the primary tumor, metastatic dissemination remains a great clinical challenge in oncology.

In the field of metal-drugs, the clinically employed Pt(II) compounds offered good results in the treatment of several primary solid tumors but were poorly effective against their metastatic spread. On the contrary, the ruthenium complexes NAMI-A (*i.e.*, (ImH)[*trans*-$RuCl_4$(dmso-*S*)(Im)], where Im = imidazole), KP1019 (*i.e.*, (IndH)[*trans*-$RuCl_4(Ind)_2$], where Ind = indazole), RAPTA-T (*i.e.*, [$RuCl_2$(PTA)($\eta^6$-toluene)], where PTA = 1,3,5-triaza-7-phosphaadamantane), and related congeners exhibited excellent antimetastatic properties but less pronounced cytotoxic activity.[1-3] Few other examples of antimetastatic metal compounds have been reported so far.[4-7] Interestingly enough, a bifunctional heterodinuclear Pt(IV)-Ru(II) prodrugs offered a combination of both cytotoxic and antimetastatic propensities.[8]

Pt(IV) antitumor drug candidates are considered prodrugs since they can be reduced in the hypoxic (and then reducing) intracellular milieu of tumor cells to the corresponding cytotoxic Pt(II) metabolite with the loss of their two axial ligands (*activation by reduction*, Scheme 1). The saturated six-coordinate octahedral geometry of low-spin $d^6$ Pt(IV) core is characterized by a higher kinetic inertness that minimizes most of the off-target effects showed by Pt(II) complexes, whose chemistry is based on moderately fast ligand exchange reactions. Suitable bioactive ligands can be coordinated to the Pt(IV) core (in the axial position, generally as carboxylate derivatives), so that the final conjugate can operate on multiple targets with greater potency. The final effect is to obtain a bifunctional, hybrid, or dual-action anticancer prodrug (*combo*) able to deliver two cytotoxic moieties (*i.e.*, a Pt(II)-based metabolite as cisplatin, and the axial bioactive ligands, Scheme 1), in the same place and at the same time, after *in vivo* reduction.[9-11]

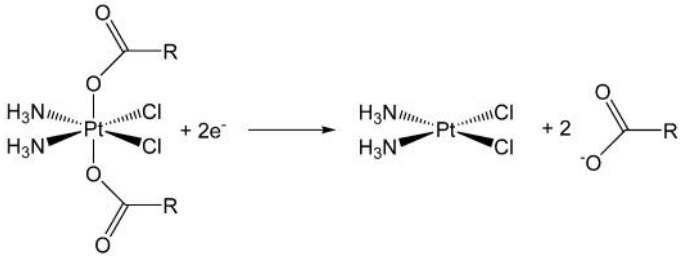


**Scheme 1**. Activation by reduction mechanism of a cisplatin-based Pt(IV) bis-carboxylato compound.

The rationale of this work was to design a Pt(IV) *combo* able to delivery to tumor cells both a cytotoxic agent (cisplatin) and an antimetastatic moiety (perillic acid, (4-isopropenylcyclohexene-1-carboxylic acid, **PA**).

Monoterpenes, largely present in the essential oils from citrus and other plants, show chemopreventive and/or chemotherapeutic properties. D-limonene, consumed by humans predominantly as an ingredient of traditional food (citrus fruits, carrots, coffee, orange, but it is also used as a safe flavoring agent in fruit juices, soft drinks, etc.), is rapidly

[a] *Dipartimento di Scienze e Innovazione Tecnologica, Università del Piemonte Orientale, Viale Michel 11, 15121 Alessandria, Italy. Corresponding author: domenico.osella@uniupo.it*
[b] *Dipartimento di Biologia e Biotecnologie "L. Spallanzani", Università di Pavia, Via Ferrata 9, 27100 Pavia, Italy.*

Electronic Supplementary Information (ESI) available: NMR, HPLC and ESI-MS characterization of the complexes and their solvation products; [$^1$H, $^{15}$N] HSQC spectra for the reduction with cell extracts; clonogenic assay; images and graphs obtained from experiments with A-549 spheroids; genes analysed with RT-qPCR. See DOI: 10.1039/x0xx00000x

metabolized by monoxygenases, belonging to the cytochrome P450 family, to oxidized products such as perillyl alcohol and **PA**, among the others.[12] Perillyl alcohol [(4-isopropenyl-1-cyclohexen-1-yl)methanol] have attracted attention because of its anticancer activity in a number of preclinical models, that pushed it in some phase I/II clinical trials.[13] Also **PA** inhibits the proliferation of A-549 and H520 lung cancer cells, increasing caspase-3 activity (the activation of caspases plays a central role in the execution-phase of cell apoptosis) and cleavage of PARP (poly(ADP-ribose)polymerase, a family of proteins involved in DNA repair and programmed cell death).[14, 15] Moreover, **PA** inhibits both farnesyltransferase (FTase) and geranylgeranyltransferase (GGTase I), the enzymes catalyzing the attachment of either a farnesyl or a geranylgeranyl isoprenoid to a protein (protein prenylation).[16] This process is essential for the cellular activity of many oncogenic proteins, including some Ras family members. As such, inhibitors of prenylation as **PA** block Ras signaling and represents a promising strategy for antitumor targeted therapy.[17-21] Finally, preclinical *in vivo* models showed that **PA** exhibits also good antimetastatic activity,[22] modulates the immune system,[23] and acts as radiosensitizer in chemoradiation therapy of head and neck cancers.[24] Importantly, combination studies revealed that exposure of the cells to **PA** sensitizes them to cisplatin: the co-administration of **PA** and cisplatin, at concentrations in the same order of magnitude, increases sensibly the potency of the Pt drug.[25]

In this framework, two Pt(IV) complexes containing one or two molecules of **PA** (**1** and **2**, Scheme 2) were synthesized and tested *in vitro* on several human tumor cell lines, including some highly chemoresistant malignant pleural mesothelioma (MPM) cells. Detailed *in vitro* biological experiments were carried out on the most promising **2** prodrug.

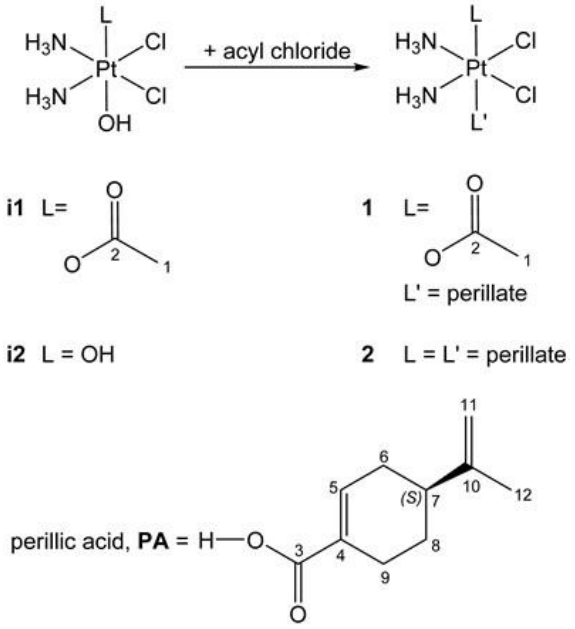


**Scheme 2**. Sketch of the Pt(IV) complexes under investigation and numbering scheme for the identification of the NMR signals.

## Results and discussion

**Synthesis and characterization of Pt(IV) bifunctional complexes.**

The Pt(IV) complexes under investigation were obtained following well-established procedures (Scheme 2). Briefly, (*SP*-4-2)-diamminedichloridoplatinum(II) (cisplatin, **CDDP**) was prepared according to the Dhara's method,[26, 27] and oxidized to the **i1** and **i2** intermediates by using $H_2O_2$ in acetic acid and in water, respectively.[28-30] Finally, the reaction of such molecules with perillyl chloride allowed the insertion of one (**1**) or two (**2**) **PA** anions in axial position with both traditional and microwave-assisted heating (see Experimental). Moreover, $^{15}$N-cisplatin was employed to prepare isotopically labeled complexes (**$^{15}$N-1** and **$^{15}$N-2**, respectively) to be used to study their reduction with cytosol.[31] All the complexes were characterized by the usual analytical techniques, such as RP-HPLC, ESI-MS, and multinuclear NMR spectroscopy using both mono- and bi-dimensional techniques (*i.e.*, correlation spectroscopy, COSY, heteronuclear multiple bond correlation, HMBC, and heteronuclear single quantum coherence spectroscopy, HSQC, to assign the whole set of signals (see ESI, Figures S1-S18).

In particular, the coordination of the axial ligands was confirmed by the shift to higher frequencies of the $^1$H and $^{13}$C NMR signals of the atoms nearer to the metal center in the Pt complexes with respect to the free carboxylates. Finally, $^{195}$Pt NMR and $^{15}$N NMR spectroscopy provide further information on the oxidation state of the metal and on the nature of the surrounding ligands.[32-36] The $^{195}$Pt NMR signals of all the complexes exhibit chemical shifts in the 1050-1250 ppm range, consistent with a "$[PtCl_2N_2O_2]$" core.[29, 37-39] The $^{15}$N NMR signals of $^{15}$N-labeled complexes **$^{15}$N-1** and **$^{15}$N-2** show chemical shifts around -40 ppm in tune with the presence of chlorides *trans* to $^{15}NH_3$ in Pt(IV) complexes.[35, 36]

Finally, RP-HPLC was used to measure lipophilicity of **1** and **2**.[40, 41] The retention time due to the partitioning between C18 chains of the stationary phase (representing the cellular membrane) and aqueous eluent (representing the water inside and outside cells) gives a parameter similar to the traditional log $P_{o/w}$ (*i.e.*, the log of the octanol/water partition coefficient) to evaluate the lipophilicity of a molecule. Therefore, the dimensionless capacity factor $k'$ ($k' = (t_R - t_0) / t_0$, where $t_R$ = retention time of the compound under investigation and $t_0$ = column dead time) of **1** and **2** was measured by using a 30/70 15 mM formic acid / methanol mixture as the eluent. As expected, **1** is less lipophilic than **2** (log $k'$ = 0.15 and 0.68, respectively), whereas both are more lipophilic than cisplatin (log $k'$ = -0.38). This higher lipophilicity is due to the presence of the **PA** molecule (log $k'$ = 0.55) as axial ligand.[42-44] Recently, some models for the prediction of the log $P_{o/w}$ values for both Pt(II) and Pt(IV) complexes have been developed and made publicly available. These models (***ASNN5 model, **http://ochem.eu/article/76903**,[45] for Pt(IV) and **http://www.vcclab.org/web/pt/**,[46] for Pt(II) complexes, respectively) were applied to the studied complexes. The trend of the experimental log $k'$ is in tune with the calculated log $P_{o/w}$: cisplatin = -2.30; **1** = 0.02; **2** = 1.62.

**Stability in solution and reduction with cytosol.**

Complexes **1** and **2** were challenged with HEPES buffer (HEPES = 4-(2-hydroxyethyl)-1-piperazineethanesulfonic acid, pH = 7.5) containing methanol to maintain the compounds in solution. Both complexes showed an excellent stability after 72 h in buffer solution (>98% evaluated by comparison of the HPLC peak areas).

The solution behavior of **1** and **2** was also investigated in cell culture medium RPMI 1640 over 72 h, using methanol as a cosolvent. Complex **1** underwent hydrolysis with the substitution of one chloride:[47-49] after 4 h (duration of the uptake experiments, see below) the degree of hydrolysis was negligible within the experimental error, whereas after 72 h the conversion reached 50% (see ESI, Figure S10). In the case of **2**, 95% of intact complex was still existing after 72 h without evident traces of solvolysis products.

The reduction of $^{15}$N-labeled complexes **$^{15}$N-1** and **$^{15}$N-2** was directly assessed in the cytosolic extract of A-549 cancer cells. The reaction was followed by [$^{1}$H, $^{15}$N] HSQC experiments: after 2 h the original signals of both Pt(IV) complexes (**$^{15}$N-1** $^{15}NH_3$ ¢ = –40.5 ppm and $^{1}$H ¢ = 6.4 ppm; **$^{15}$N-2** $^{15}NH_3$ ¢ = –36.8 ppm and $^{1}$H ¢ = 6.2 ppm) disappeared. In the meantime, those of cisplatin growth ($^{15}NH_3$ ¢ = –67.6 ppm with satellite peaks at -63.5 ppm e -69.9 ppm, $^{1}J_{Pt\text{-}N}$ = 327 Hz and $^{2}J_{Pt\text{-}H}$ = 69 Hz; $^{1}$H ¢ = 4.0 ppm, see ESI, Figures S19-S22).[50, 51] Similar experiments performed by Gibson *et al.* with aqueous extract of some human cancer cells gave similar reduction rates.[51] Comparing the contact time between the complexes and cytosol (2 h) with the time employed in the biological tests (72 or 24 h, see below), and considering also the stability in cell culture media, one can affirm than **1** and **2** enters intact into the cells and, once in the cytosol, exert their activity essentially by means of their metabolites, namely **CDDP** and **PA**.

**Antiproliferative activity and cytotoxicity.**

Compounds **1** and **2** were tested on several human cancer cell lines, namely A2780 (ovarian endometrioid adenocarcinoma), NT2/D1 (embryonal carcinoma), A-549 (lung adenocarcinoma), HCT116 (colon carcinoma), HT29 (colon adenocarcinoma), MCF7 (breast adenocarcinoma). To this panel, three malignant pleural mesothelioma MPM cell lines were added, namely BR95 (epithelioid phenotype), MG06 (biphasic or mixed phenotype), and MM98 (sarcomatoid phenotype) together with its cisplatin-resistant subline MM98R and a primary human mesothelial cell (HMC) line.

The $IC_{50}$ (*i.e.*, the concentration of drug which reduces cell growth by 50%) values were determined by the resazurin cell viability assay. In addition, the resistance factor RF (*i.e.*, the ability to bypass cisplatin-resistance, RF = $IC_{50}$ (MM98R) / $IC_{50}$ (MM98)) and the selectivity index SI (*i.e.*, the ability to discriminate between normal and malignant cells belonging to the same or similar tissue, SI = $IC_{50}$ (HMC) / mean $IC_{50}$ (BR95, MG06, and MM98)) were calculated.[52] Cisplatin and **PA** were added to the series for comparison purposes. All the data are reported in Table 1.

**Table 1.** Half-maximal inhibitory concentrations ($IC_{50}$, μM) of **CDDP**, **PA**, **1**, and **2**.[a]

| | A2780 | NT2/D1 | A-549 | HCT 116 | HT-29 | MCF-7 | BR95 | MG06 | MM98 | MM98R | HMC |
|---|---|---|---|---|---|---|---|---|---|---|---|
| **CDDP** | 0.460±0.110 | 0.106±0.039 | 3.60±0.90 | 2.30±0.30 | 2.83±0.33 | 6.50±0.90 | 6.20±0.90[b] | 4.10±1.50[b] | 3.20±1.20[b] | 19.4±1.2[b] (6.1) | 6.7±1.3[b] [1.5] |
| **PA** | 639±140 | 1265±318 | 1043±496 | 1346±469 | 1770±398 | 2660±523 | 974±412 | 919±355 | 3210±879 | 2520±654 (0.8) | 2850±380 [1.7] |
| **1** | 0.056±0.014 | 0.063±0.034 | 0.575±0.147 | 0.304±0.129 | 1.06±0.36 | 0.810±0.301 | 1.73±0.52 | 2.34±0.91 | 0.501±0.103 | 0.304±0.101 (0.6) | 4.42±0.73 [2.9] |
| **2** | 0.0022±0.0004 | 0.0037±0.0011 | 0.0081±0.0036 | 0.011±0.003 | 0.010±0.002 | 0.041±0.004 | 0.150±0.051 | 0.094±0.018 | 0.028±0.005 | 0.031±0.013 (1.1) | 0.290±0.092 [3.2] |

[a] The values were measured after 72 h of treatment on A2780 (ovarian endometrioid adenocarcinoma), NT2/D1 (embryonal carcinoma), A-549 (lung adenocarcinoma), HCT 116 (colon carcinoma), HT29 (colon adenocarcinoma), MCF7 (breast carcinoma), BR95 (epithelioid MPM), MG06 (biphasic MPM), and MM98 (sarcomatoid MPM) together with its cisplatin-resistant subline MM98R and primary human mesothelial cell (HMC) line. Data are mean ± standard deviation (sd) of at least three independent replicates, performed in triplicate. Numbers in round parenthesis are the resistance factor RF = $IC_{50}$ (MM98R) / $IC_{50}$ (MM98); numbers in square brackets are the selectivity index SI = $IC_{50}$ (HMC) / mean $IC_{50}$ (BR95, MG06, MM98). [b]Data from ref. [53].

The Pt(IV) complexes **1** and **2** were more active than cisplatin on all the cell lines under study by one or two orders of magnitude, respectively. The cytotoxicity of **1** fall in the low μM range, whereas **2** acts in the nM interval. On the contrary, **PA** is active on all cancer cell lines at mM concentrations. The RF value is quite good for **1** and **2** (around 1 as compared with 6.1 of cisplatin itself) as often occur for several moderately lipophilic Pt(IV) prodrugs.[42, 54-56] Interestingly enough, the gold standard chemotherapeutic treatment of the very aggressive MPM is based on cisplatin.[54]

On the contrary, the SI is only moderately higher for **1** and **2** (around 3) than for cisplatin (1.5); unfortunately, most of the Pt-based antitumor drugs are poorly selective.

Prodrug **2** exhibited an antiproliferative activity one or two order of magnitude higher than **1,** having the former higher lipophilicity and releasing after reduction two equivalents of **PA** instead of one. Therefore, the whole set of *in vitro* biological experiments were focused on the activity of **2** on A-549 cell line, which represent a good model for metastatic propensity.[57]

To evaluate drug sensitivity of cancer cells there are several methods, which essentially fall into two groups: those that measure viability (as the resazurin assay employed for $IC_{50}$ evaluation) and those that assess cytotoxicity as the clonogenic (or colony-forming) assay, which evaluates the ability of cells to proliferate again after the drug treatment (typically 72 h).[58] For this purpose, $1\times10^3$ A-549 cells were treated for 72 h with equitoxic concentrations of **CDDP**, **PA**, **1** and **2**, rounded as 5 μM, 1 mM, 0.5 μM, and 10 nM, respectively (hereafter the term "72 h-equitoxic" refers to the above concentrations). Then, the culture medium was removed and substituted by a fresh one. The cells were maintained without drug for a week (recovery), and, finally, the living cells were stained with crystal violet (see ESI, Figure S23). Survivors from the 72-h treatment with **PA** partially recovered their proliferative activity, and the result was the formation of about 50% of colonies, with respect to the control. On the contrary, after the treatment with the three Pt complexes there was a complete absence of colonies. Noteworthy, the cytotoxic activity of the cisplatin moiety is increased in **2**, since the same result is achieved at a concentration three time lower. The clonogenic assay was performed also on HCT-116 cells with the same protocol used for A-549, and the results were very similar (see ESI, Figure S23).

The activity of **2** was also evaluated by employing multicellular tumor spheroids (MCTS) as 3D culture model. In fact, MCTS simulate the poorly vascularized tumors and allow to evaluate the drug penetration in the necrotic core. Moreover, MCTS permit to distinguish between antiproliferative activity (growth decrease or arrest for a relatively short period and then re-growth) and cytotoxic activity (no re-growth at all) with the advantage of the extension of the viability experiments for longer times (approximately up to two weeks).[59-63] MCTS obtained from A-549 cancer cells were treated for 72 h with 72 h-equitoxic concentrations of cisplatin, **PA**, **1** and **2**, followed by 11 d recovery in fresh medium.[56] Figure 1 shows that **PA** caused a moderate effect on the dimension (volume) of MCTS (see ESI, Figure S24 for MCTS images and Figure S25 for complete data). The Pt drugs halve the MCTS size (cisplatin and **1**) or strongly inhibit the growth (**2**). Finally, treatment with **2** at a concentration $10\times IC_{50}$ (100 nM) caused the MCTS to totally disaggregate.

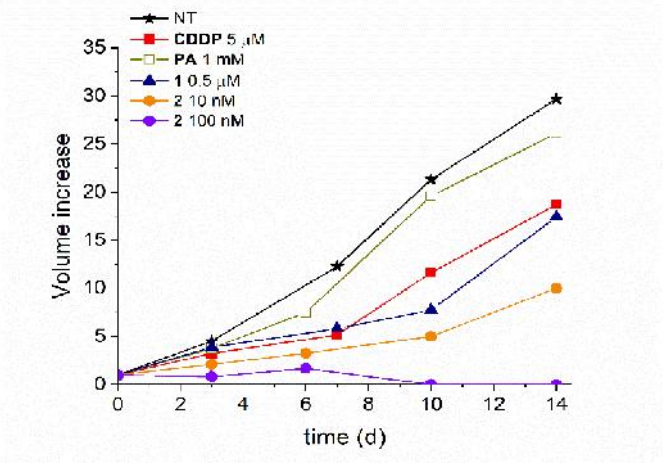


**Figure 1.** Multicellular Tumor Spheroids (MCTS) growth inhibition. MCTS obtained from A-549 cells were treated with 72 h-equitoxic concentrations ($1\times IC_{50}$) of cisplatin, **PA**, **1**, and **2** from day 0 to day 3, then followed in drug-free medium (recovery). In the case of **2**, also the results obtained after $10\times IC_{50}$ treatment are reported. Data are mean of volume fold increase (*vs.* untreated MCTS, NT) of at least 3 independent replicates; error bars are omitted for clarity.

In conclusion, the data obtained employing MCTS confirm those of the clonogenic test, that is the high cytotoxic propensity of 2 on A-549 cells, taking into account that the efficiency of a given drug on 3D MCTS is intrinsically minor than that on 2D cell monolayer.[64]

### Combination index (CI)

The combination index (*CI*) was used to evaluate the pharmacological interaction between the two metabolites (*i.e.*, cisplatin and **PA**) produced upon *in vitro* reduction by **2**.[65, 66] This method evaluates the effect of two drugs and quantifies synergism or antagonism by determining how the combination effect differs from the simple additive effect. After solving the equation proposed by Chou and Talalay, the resulting *CI* values point out an additive (*CI* = 1), synergistic (*CI* < 1), or antagonistic (*CI* > 1) effect of the interacting drugs (see Experimental).

Figure 2 indicates that cisplatin and **PA** have a moderate synergistic action on A-549 in the whole range of concentrations employed, so that the two metabolites released within the cells by **2** are expected to increase each other's effectiveness.

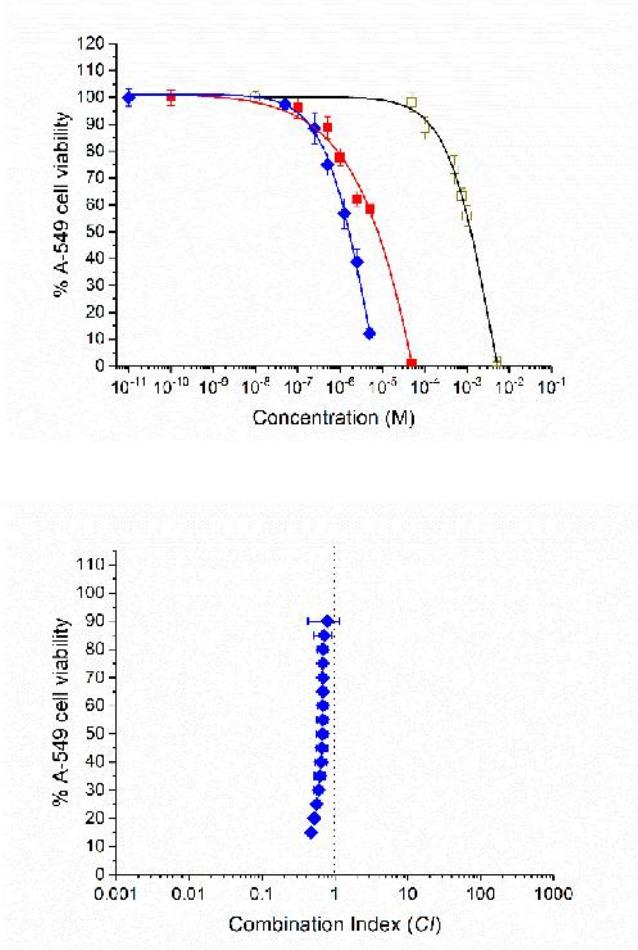


**Figure 2**. Concentration–response curves (top) of A-549 cells challenged for 72 h with **PA** (empty squares), CDDP (red squares), and mixture 1:600 CDDP/(2×**PA**) according to their 72 h-$IC_{50}$ values (blue rhombus). Data are mean ± sd of a representative experiment. Residual viability was assessed by means of the resazurin reduction assay and data were fitted with a four-parameter sigmoidal function. Combination index (*CI*) plot (bottom) of the mixture 1:600 CDDP/(2×**PA**). Residual viability data were compared to those obtained for cisplatin and **PA** to obtain the value (*CI* < 1: synergism; *CI* ≅ 1 additive effect; *CI* > 1 antagonism).

**Cell uptake and DNA platination.**

Cellular accumulation and DNA platination of **2** was evaluated by means of ICP-MS technique after 4 h and 24 h of continuous treatment (CT) and after 4 h of treatment followed by 20 h of recovery without the drug in the culture medium (R) (Figure 3). Cisplatin and **1** were tested as reference compounds.

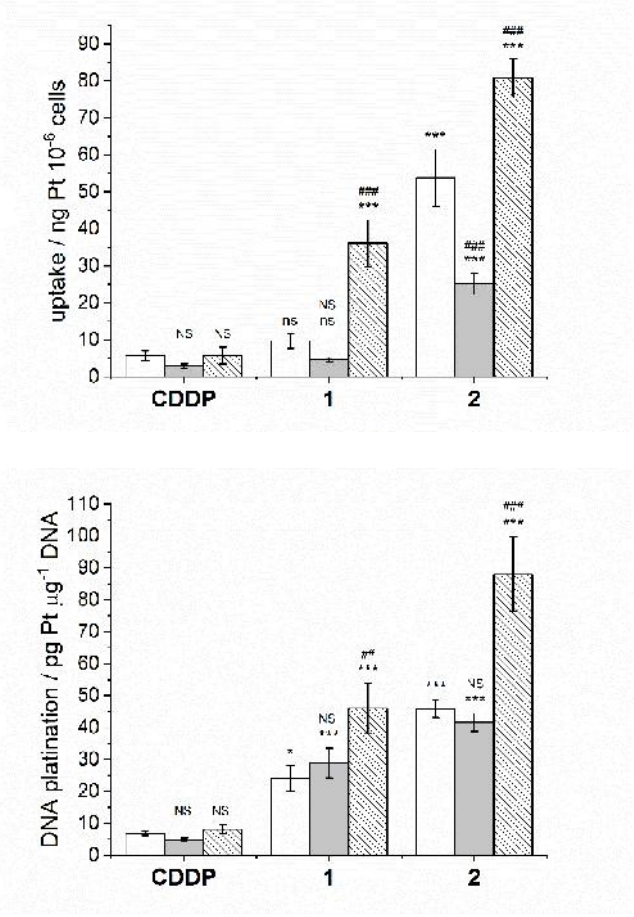


**Figure 3**. Cell uptake (top) and DNA platination (bottom) of cisplatin (**CDDP**), **1**, and **2** in A-549 cells treated for 4 h CT (white bars), 4 h CT followed by 20 h R (grey bars), or 24 h CT, patterned bars) at 10 µM concentrations. Statistical analysis: **CDDP** *vs.* **1** or **2** (same treatment conditions) ns = not significant, (*) p < 0.05, (**) *p* < 0.01, (***) *p* < 0.001; 4 h CT *vs.* 4 h CT + 20 h R or 24 h CT (same compound) NS = not significant, (#) *p* < 0.05, (##) *p* < 0.01, (###) *p* < 0.001.

As expected, the Pt uptake follows the trend of lipophilicity (**2** > **1** > cisplatin) and the DNA platination is roughly proportional to the Pt accumulation.

According to the concept of *synergistic cellular accumulation*, in dicarboxylate Pt(IV) complexes the combination of a hydrophilic cisplatin (negative log $P_{o/w}$) with two amphiphilic **PA** anions (at physiological pH), which neutralize the positive charge on Pt(IV) core and protrude toward exterior their aliphatic chains, generates a very lipophilic conjugate. This *combo* prodrug enters cells *via* passive diffusion more efficiently than the free components cisplatin and **PA**, increasing their intracellular concentrations with respect to a simple co-administration in separate form. This explains the large increase in activity ($1/IC_{50}$) on passing from cisplatin to **2**, increase that largely exceeds the moderate synergistic effect found for the mixture of its free components.

Interestingly enough, in the 4 h CT + 20 h R experiment, the DNA platination did not significantly decrease during the recovery period, indicating a high persistence of the lipophilic Pt(IV) prodrugs as previously found.[67] The DNA platination carried out

by **2** was by far the highest among the Pt complexes under investigation, paralleling the highest antiproliferative activity.

**Apoptosis induction.**

The cytotoxic effect of cisplatin is mainly related to the formation of intra- and interstrand DNA cross-links by the active electrophilic agent "$[Pt(NH_3)_2]^{2+}$" that finally leads to apoptosis.[68] The cysteinyl aspartate-specific protease (caspase) cascade is activated during apoptosis induction. The process of apoptosis is orchestrated by the activation of "executioner" caspases (caspase 3 and caspase 7), that cleave specific substrates within the cell to produce the changes associated with apoptosis. Therefore, the activity of caspases 3/7 after treatment with cisplatin, **PA** and **2** was investigated at several concentrations (Figure 4). Both Pt-complexes significantly increased caspase 3/7 activity, albeit **2** produces this effect at a concentration about 240 times lower than that of cisplatin. This scenario is consistent with higher Pt uptake of **2** with respect to cisplatin. In order to check whether fluorescence is specifically associated to caspase activity, the experiments were repeated in the presence of the Ac-DEVD-CHO inhibitor, able to quench fluorescence due to caspases.

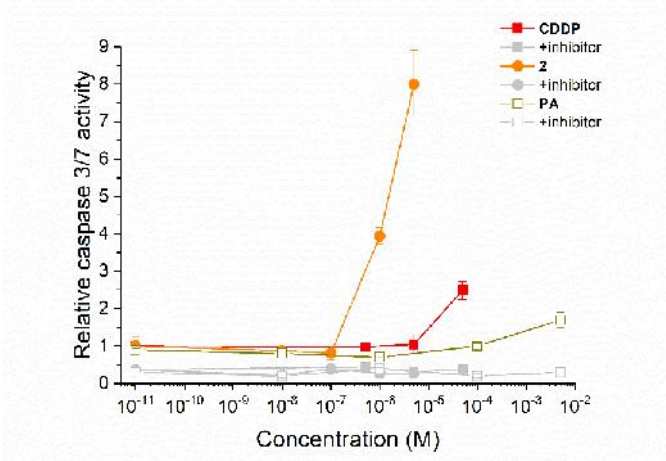


**Figure 4**. Caspase 3/7 activity assay. A-549 cells were treated with increasing concentrations of **CDDP**, **PA**, and **2**. The caspase 3/7 fluorogenic substrate Ac-DEVD-AFC was added to all wells. Data were normalized over the untreated control and reported as fold activity. The grey lines were obtained from experiments repeated in the presence of the Ac-DEVD-CHO inhibitor.

**Gene modulation evaluated by Quantitative Reverse Transcription PCR (RT-qPCR).**

To shed more light on the underlying biochemical mechanisms triggered upon drug challenge, a Quantitative Reverse Transcription PCR (RT-qPCR) analysis has been carried out. Preliminarily, since in this and in the following experiments A-549 cells were treated for 24 h, new $IC_{50}$ values were calculated for cisplatin, **PA**, and **2** (rounded as 50 μM, 1 mM, and 1 μM, respectively) at this time point. The 24 h $IC_{50}$ values are obviously higher for cisplatin and **2** (*i.e.*, lower cytotoxic activity *vs.* 72 h treatment), as expected for any genotoxic Pt-drug that requires some cell cycles to manifest the maximum effect. Hereafter, the term "24 h-equitoxic" refers to the above concentrations.

To further confirm the apoptosis induction caused by **2**, the variation of the expression of three genes because of drug challenge was evaluated (Figure 5). In particular, the intrinsic apoptotic pathway is regulated by the B cell leukemia-2 gene product (BCL-2) family. This family contains the pro-apoptotic BAX and BAD, and anti-apoptotic BCL-2 members, that have been analyzed here.[69]

The expression of two other genes was investigated: CDKN1A (cyclin-dependent kinase inhibitor 1A) and TP53 (tumor protein 53). The p21 protein encoded by CDKN1A was first described as a potent inhibitor of cell proliferation and DNA replication.[70] Interestingly, Agrawal and Gadgil published a meta-analysis of gene expression changes upon treatment of A-549 cells with several anti-cancer drugs revealing that CDKN1A is upregulated in four out of seven drug treatments considered.[71] Thus, in A-549 cells the expression of p21 testifies the antiproliferative effect of **2**.

The most frequently mutated gene in many human tumors is TP53, encoding the p53 protein. One of the best-understood activity of the p53 is the promotion of cell cycle arrest and apoptosis. For these and other reasons, TP53 was classified as a "tumor suppressing gene" (TSG).[72, 73]

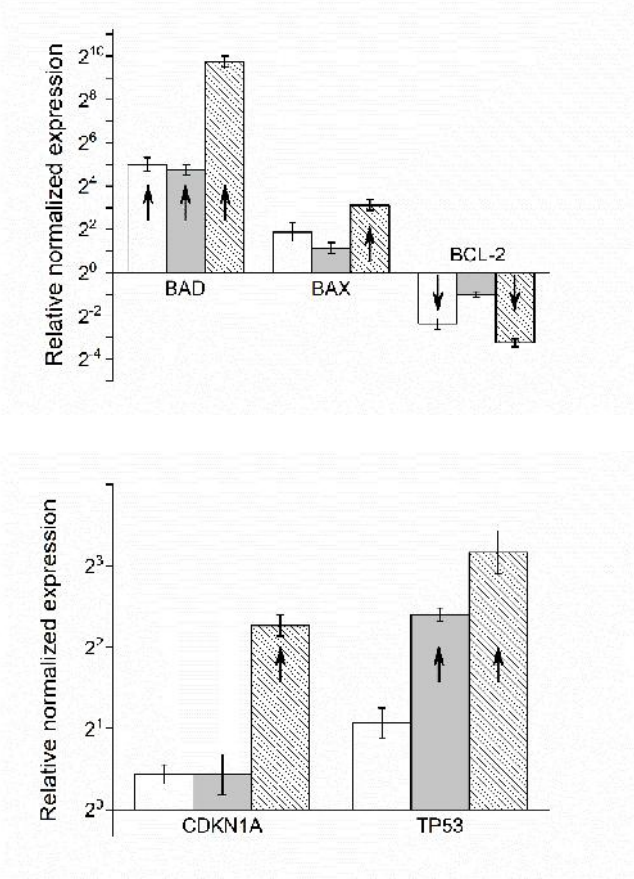


**Figure 5**. Relative gene expression of BAD (pro-apoptotic), BAX (pro-apoptotic), BCL-2 (anti-apoptotic), CDKN1A (p21 encoding gene) and TP53 (p53 encoding gene) in A-549 cells following 24 h treatments with 24 h-equitoxic concentrations of cisplatin (white bars), **PA** (grey bars), and **2** (patterned bars). The RT-qPCR experiment was performed in triplicate, and results were normalized to references genes in untreated control. The arrows indicate the upregulated (arrow up) or downregulated (arrow down) gene

expression with respect to internal threshold value as determined by the CFX Manager software.

Cisplatin, **PA**, and **2** showed a similar effect on all the genes. Their major influence is in the upregulation of pro-apoptotic BAD and, to a lesser extent, the downregulation of anti-apoptotic BCL-2. These data are in tune with the enhanced induction of apoptosis shown by **2** on A-549 cancer cells. Moreover, upregulation of both CDKN1A and TP53 induced by **2** was higher than that induced by cisplatin and **PA** alone.
Altogether, **2** showed the highest effect (*vs.* cisplatin and **PA**) on all the genes at equitoxic concentrations, pointing out an advantage in the combination of the two moieties in the *combo* assembly. In particular, the observed upregulation of TP53 seems to be strongly related to the presence of **PA** in the structure of **2**.

**Loss of mitochondrial transmembrane potential and ROS generation.**

Apoptosis can be triggered through the extrinsic (receptor-mediated) and the intrinsic (mitochondrial-mediated) pathways, both converging on the same terminal (execution pathway). For their position in the cascade, activation of caspase 3/7 is a general indicator of apoptosis progression, and other tests are necessary to discriminate between extrinsic or intrinsic pathways.
In the intrinsic pathway, the functional consequence of pro-apoptotic signaling is the loss of mitochondrial transmembrane potential $\Delta\Psi_M$ (depolarization) and subsequent membrane permeabilization, with release of cytochrome c in the cytoplasm and the production of reactive oxygen species (ROS).
Several reports have proved that metal-based drugs potentiate their anti-tumor efficiency through increasing generation of ROS.[74-76] This holds true for cisplatin and even more for Pt(IV) prodrugs, as they furthermore act as intracellular oxidizing agents. This process in turn drops the mitochondrial transmembrane potential in a sort of vicious cycle.[77]
The lipophilic cationic dye, 5,5',6,6'-tetrachloro-1,1',3,3'-tetraethylbenzimidazolylcarbocyanine iodide (JC-1), has been developed to "measure" $\Delta\Psi_M$. In cells with high mitochondrial transmembrane potential (healthy cells), JC-1 enters the energized mitochondria and form aggregates that show intense red fluorescence. Unhealthy or apoptotic cells have low $\Delta\Psi_M$ and JC-1 remains in the monomeric form, which shows only green fluorescence. The ratio of green to red fluorescence is dependent only on the membrane potential: higher the ratio, the higher is the polarization of mitochondrial membrane. Figure 6 shows the % red/green ratio of A-549 cells treated with cisplatin, **PA** and **2**. Only **2** induced a statistically significant depolarization of mitochondria.

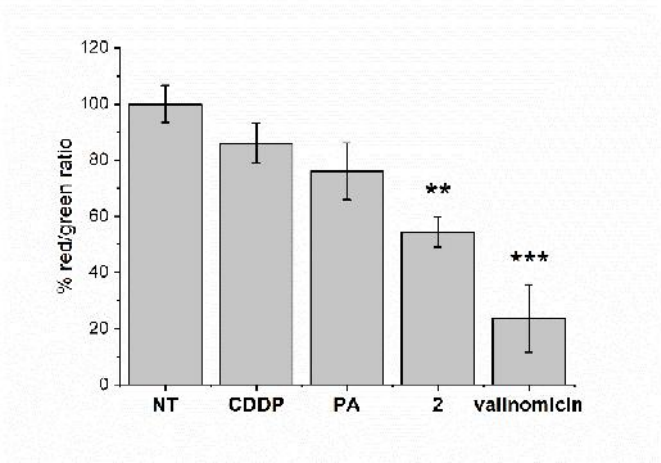


**Figure 6**. Assay of A-549 cells mitochondrial membrane potential with JC-1 staining method. Cell were treated for 24 h with 24-h equitoxic concentrations of **PA** (1 mM), cisplatin (50 μM), and **2** (1 μM) and quantitative analysis of % ratio of red/green fluorescent intensity is reported as mean ± sd of triplicates. NT = non-treated. Valinomycin was used as the positive control. Statistical analysis: NT *vs.* treated samples (**) $p < 0.01$; (***) $p < 0.001$.

The quantification of ROS was assessed by using the 2',7'-dichlorodihydrofluorescein diacetate ($H_2$DCF-DA) probe that passively diffuses into cells where is retained after cleavage by intracellular esterases. The resulting nonfluorescent probe is converted into the highly fluorescent 2',7'-dichlorofluorescein (DCF) upon oxidation by ROS. After 24 h-equitoxic treatment of A-549 cells with **2**, cisplatin, and **PA**, a general growth in the ROS level was observed for all compounds. The increase caused by **2** was statistically more significant with respect to cisplatin and **PA** (Figure 7). This is clearly related to the strong decrease of the mitochondrial membrane previously observed after challenging A-549 cells with **2**.

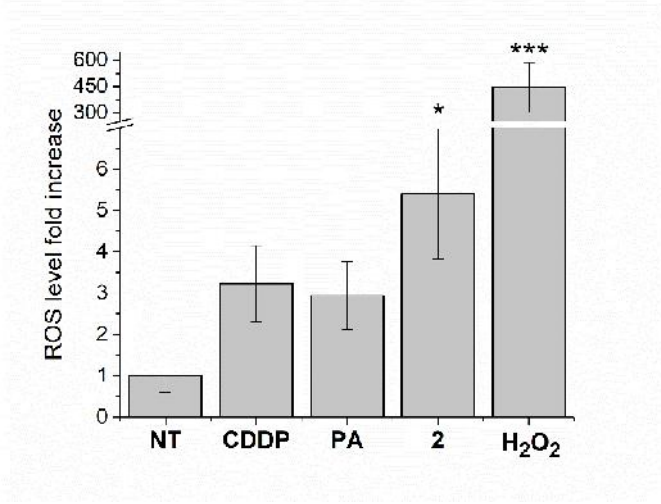


**Figure 7.** Assay of ROS production in A-549 cells with the 2',7'-dichlorodihydrofluorescein diacetate assay kit. Cell were treated for 24 h with 24 h-equitoxic concentrations of **PA,** cisplatin and **2**. $H_2O_2$ was used as the positive control. The fold increase of ROS *vs.* NT is reported as mean ± sd of triplicates, (*) $p < 0.05$.

**Antimetastatic effect.**

Literature data show that administration of monoterpenes, such as limonene and **PA**, to C57BL/6 mice with lung metastasis induced by B16F-10 melanoma cells, resulted in a remarkable reduction in the metastatic tumor nodule formation. These results, together with the analysis of several biochemical parameters and histopathological studies, indicated that **PA** could inhibit the metastatic progression *in vivo*.[22]

To test if **2** could cause a widespread antimetastatic effect, the transwell migration and invasion assay was performed. The classic migration detection system uses a plastic chamber containing at one end a porous membrane. This chamber is suspended over a larger well, which may contain medium and/or chemo-attractants. Cells are placed inside the chamber and allowed to migrate through the pores to the other side of the membrane, where they are stained and counted after 24 h. This test can measure the ability of a cell to migrate from its primary site. The assay can be easily modified to perform the cell invasion assay, depositing on the top of the membrane, a layer of Matrigel™. Matrigel is a gelatinous protein mixture derived from mouse tumor cells that is commonly used to simulate the extracellular membrane matrix. Invasive cells secrete proteases that enzymatically degrade the matrix and enable invasion through the membrane pores.[78, 79]

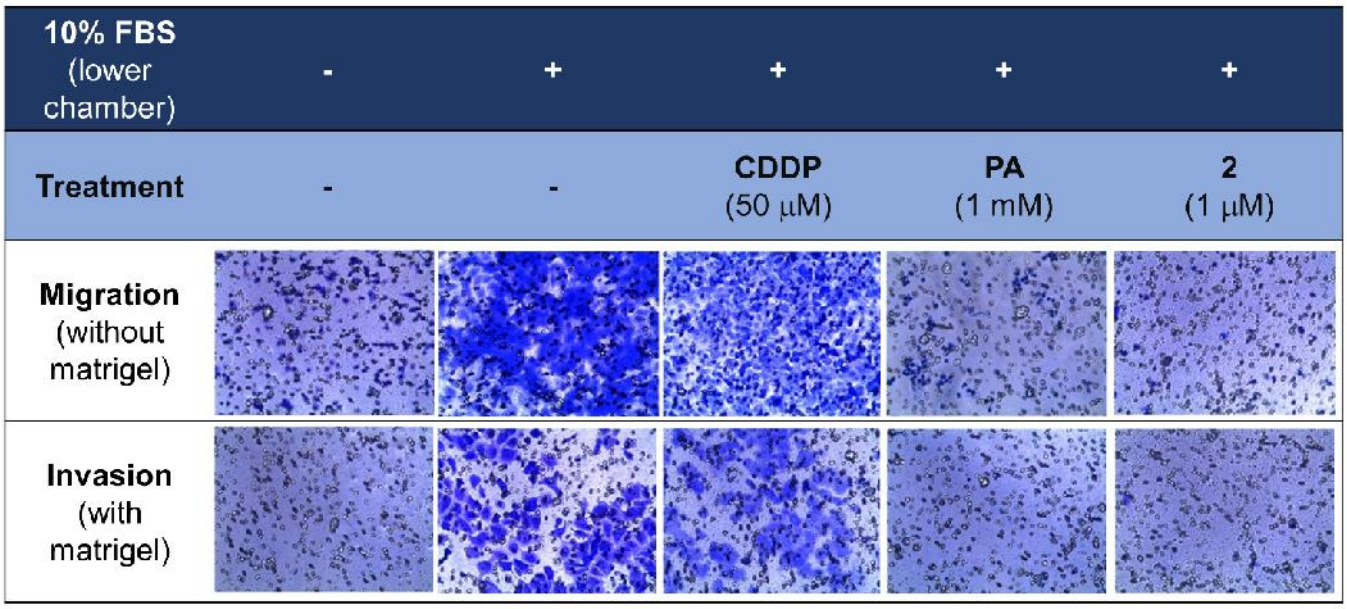


**Figure 8**. Representative pictures of the transwell assay. A-549 cells were treated with 24 h-equitoxic concentrations of **CDDP** (50 μM), **PA** (1 mM) and **2** (1 μM) for 24 h and the invading cells, stained with crystal violet, were photographed under a light microscope. FBS-free (top row of images) and FBS-containing (bottom row of images) medium was added to the lower chamber to simulate the migration and invasion control conditions, respectively.

Figure 8 shows that A-549 cells were not only able to migrate (first column in the figure, top photo), but also to invade (bottom photo) the surroundings. This movement is strongly enhanced by the presence of fetal bovine serum (FBS) as chemoattractant in the lower chamber (second column). Cisplatin treatment was almost unable to reduce both migration and invasion (third column). On the contrary, both **PA** and **2** at their 24 h-equitoxic concentrations strongly reduce the presence of cells in the collecting chamber, restoring the control conditions (fourth and fifth columns *vs.* second or first ones, respectively) in a very similar way. Remarkably, the reduction of invasion is observed for **2** at a concentration three orders of magnitude lower than that of **PA**. The synergistic accumulation effect previously described plays an important role.

The wound healing assay was also performed. In this test, a "scratch" is created in a cell monolayer; then, images at the beginning and during cell migration to close the wound are acquired. The comparison of the images permits to quantify the migration rate of the cells in the presence and absence of a drug.[80] The results obtained (Figure 9) show that there was a minor scratch closure in the samples treated with **2** and **PA**, compared to the control and even to the cisplatin-treated cells (at their 24 h-equitoxic concentrations). The treatment with **2** and **PA** induces a better anti-migration effect than that with cisplatin, confirming the antimetastatic propensity of the **PA** component.

Noteworthy, compound **2** is one of the few examples so far reported in literature of Pt complexes showing this behavior.[8, 81, 82]

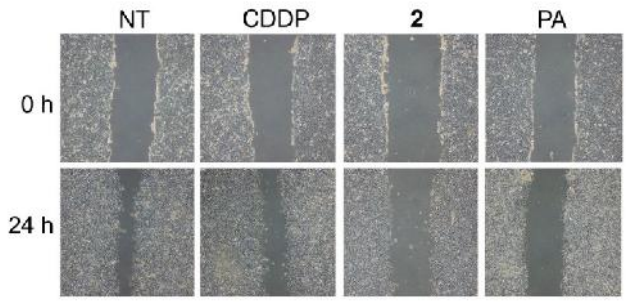

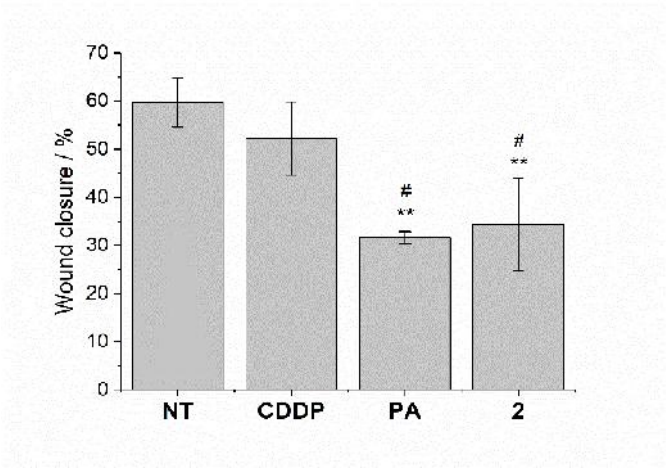


**Figure 9**. Wound healing assay: Images of scratches obtained with A-549 cells at time point 0 h for different experimental conditions (top panel). The scratches after 24 h (NT) and after 24 h-CT to the various treatments with cisplatin, **2**, and **PA** at their 24-h equitoxic concentrations, respectively (bottom panel). The histogram shows the data of the average percentage of wound closure obtained from three measurements inside the slide of each experimental condition. Statistical analysis: NT *vs.* treated samples (**) $p < 0.01$; CDDP *vs.* **2** or **PA** (#) $p < 0.05$.

**Immunocytochemical reactions for Active Cdc42.**

Finally, further insights on the biological mechanism of **2** were obtained by means of immunofluorescence analysis following the activity of Cdc42 in the A-549 cells subjected to the scratch test. Cdc42 is a member of the Rho GTPase family and it is involved in cell-to-cell adhesion and formation of cellular protrusions, which allows the cell to move directionally; for this reason, it can be used as a migration marker.[83-85]

The analysis was focused on the area near the scratch, where significant differences are expected. After treatment with **2** (1 μM concentration), as well as with **PA** (1 mM) exposure, the fluorescence optical density (OD) for active Cdc42 decreased as compared to the control, and even as compared to cells treated with 50 μM **CDDP**. This scenario indicates once again the role of **PA** in the antimetastatic activity of **2**.

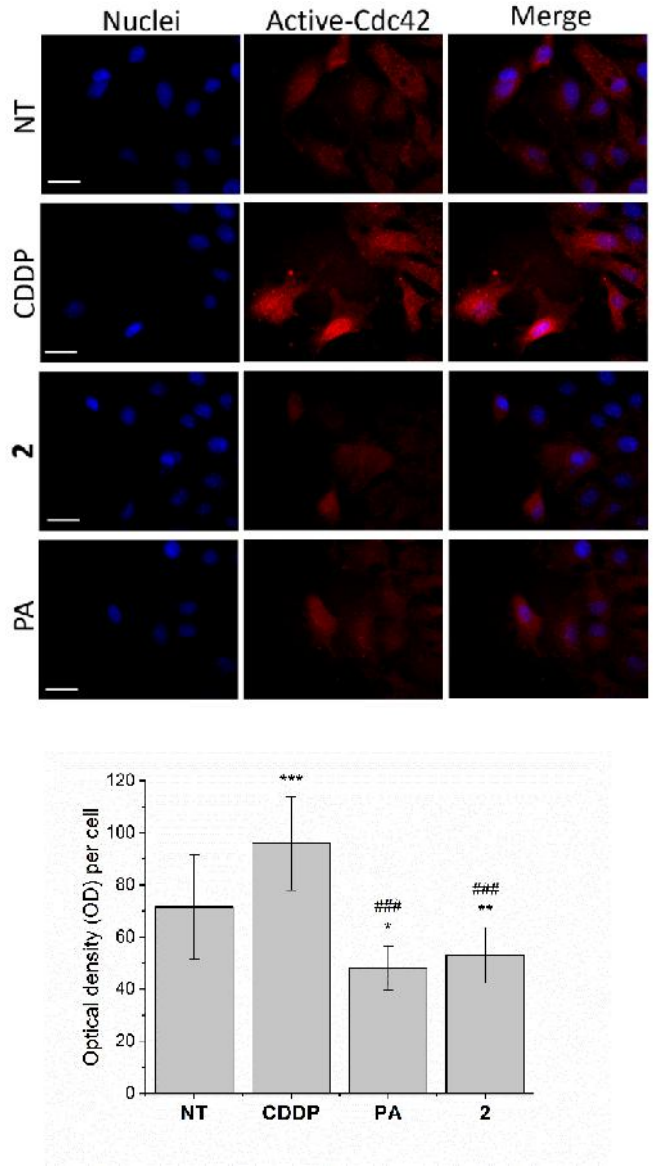


**Figure 10.** Active-Cdc42 immunolabelling A-549 cells in different experimental conditions near the scratch area. Micrographs show Active-Cdc42 (red fluorescence) immunostaining at 24 h after scratching. Nuclei were counterstained with Hoechst 33258 (blue fluorescence). Bar: 40 μm. Histogram reported the medium OD values per cell of Active-Cdc42, evaluated after treatment with the compounds under investigation. Statistical analysis: NT *vs.* treated samples (***) $p < 0.0001$; (**) $p < 0.001$; (*) $p < 0.01$; **CDDP** *vs.* **2** or **PA** (###) $p < 0.0001$.

## Experimental

**General procedures**

All the chemicals (Sigma Aldrich-Merck or Alfa Aesar-Thermo Fisher Scientific, except where otherwise specified) were used as received and without further purification. The reactions under microwave irradiation were performed by using a CEM Discover® SP System equipped with a focused single mode and self-tuning cavity, an air-cooling system, an automated power control based on temperature feedback, supplying power in 1 W increments from 0 to 300 W.

The purity of all compounds was determined using an analytical C18 Phenomenex Phenosphere-NEXT (5-μm, 250×4.6 mm ID) column on a Waters HPLC-MS instrument (equipped with Alliance 2695 separations module, 2487 dual lambda absorbance detector, and 3100 mass detector). The UV-visible detector was set at 210 nm. Mass spectra were recorded using source and desolvation temperatures set to 150 and 250 °C, respectively, with nitrogen used both as a drying and as a nebulizing gas. The cone and the capillary voltages were usually +30 V (positive ion mode) and 2.70 kV, respectively. Quasi-molecular ion peaks $[M+H]^+$ were assigned on the basis of the *m/z* values and of the simulated isotope distribution patterns. Compounds **1**-**2** and their $^{15}N$ labeled forms were confirmed to have greater than 98% purity.

The NMR spectra were measured on a NMR-Bruker Avance III operating at 500 MHz ($^1H$), 125.7 MHz ($^{13}C$) and 107.2 MHz ($^{195}Pt$ with a spectral window of 2000 ppm), respectively. $^1H$ and $^{13}C$ NMR chemical shifts were reported in parts per million (ppm) referenced to solvent resonances (the numbering scheme for the identification of the NMR signals is reported in Scheme 2). $^{195}Pt$ NMR spectra were recorded using a solution of $K_2[PtCl_4]$ in saturated aqueous KCl as the external reference. The shift for $K_2[PtCl_4]$ was adjusted to -1628 ppm from $Na_2PtCl_6$ (¢ = 0 ppm). $^{15}N$ NMR spectra were recorded using a solution of $^{15}NH_4Cl$ in 1 M HCl as the external reference. [$^1H$, $^{15}N$] HSQC spectra (Heteronuclear Single Quantum Correlation) were obtained with the standard Bruker sequence hsqcetgpsiz with 0.2 s acquisition time, 8 scans, 1.3 s relaxation delay, and 128 $F_1$ points. DEPT-45 (Distortionless Enhancement by Polarization Transfer) spectra were recorded with 100 scans, 3.5 s relaxation delay, 0.5 s acquisition time and 75 Hz for $^1J_{15N,\,1H}$.

#### Synthesis ans characterization of the complexes

Complexes (*OC*-6-44)-acetatodiamminedichloridohydroxido-platinum(IV), **i1**,[29] and (*OC*-6-33)-diamminedichlorido-dihydroxidoplatinum(IV), **i2**,[30] were prepared according to were prepared according to already published procedures.

**Synthesis of the 4-isopropenylcyclohexene-1-carbonyl chloride (perillyl chloride).** Perillic acid (4-isopropenylcyclohexene-1-carboxylic acid, **PA**, 1 eq) was dissolved in dichloromethane and one drop of dimethylformamide (DMF), as catalyst, was added. While the solution was stirring, oxalyl dichloride (5 eq) was added dropwise and effervescence was observed. The reaction mixture was stirred overnight at room temperature. The solvent and excess chloride were removed under reduced pressure (60 °C) to quantitatively yield perillyl chloride (4-isopropenylcyclohexene-1-carbonyl chloride), the acyl chloride of **PA**, as a yellow/orange oil. $^1H$ NMR (500.13 MHz, DMSO-$d_6$): ¢ 1.48–1.54 (m, 1H, H8), 1.75 (s, 3H, H12), 1.91–1.94 (m, 1H, H8'), 2.19–2.32 (m, 3H, H6, H7 and H9), 2.47–2.53 (m, 2H, H6' and H9'), 4.72 (br. s, 1H, H11), 4.79 (br. s, 1H, H11'), 7.43–7.44 (m, 1H, H5) ppm. $^{13}C$ NMR (125.76 MHz, DMSO-$d_6$): ¢ 20.8 (C12), 25.6 (C9), 26.9 (C8), 32.0 (C6), 39.7 (C7), 109.9 (C11), 135.0 (C4), 147.9 (C10), 149.8 (C5), 168.1 (C3) ppm.

**Synthesis of complex 1.** The oily acyl chloride of **PA** previously obtained ($6.65\times10^{-3}$ mol, 5 eq) was dissolved in anhydrous acetone (3 mL) and added to a suspension of complex **i1** (0.05 g, $1.33\times10^{-4}$ mol, 1 eq) in anhydrous acetone (2 mL). Excess pyridine (50 μL) was added dropwise to the reaction mixture, which was then stirred, heated up to 70°C in a round bottomed flask equipped with a reflux condenser and left overnight. The bright yellow/orange solution was evaporated under reduced pressure and the resulting oil was treated with hexane, diethyl ether and finally water to yield 0.045 g (64%) of a yellow powder for complex **1**. $^1H$ NMR (500.13 MHz, DMSO-$d_6$): ¢ 1.33–1.36 (m, 1H, H8), 1.71 (m, 3H, H12), 1.75–1.78 (m, 1H, H8'), 1.91 (s, 3H, H1), 2.02 (m, 1H, H6), 2.05 (m, 1H, H7), 2.08 (m, 1H, H9), 2.23–2.27 (m, 1H, H6'), 2.31–2.34 (m, 1H, H9'), 4.71 (br. s, 1H, H11), 4.73 (br. s, 1H, H11'), 6.54 (m, 6H, N$H_3$), 6.69 (m, 1H, H5) ppm. $^{13}C$ NMR (125.76 MHz, DMSO-$d_6$): ¢ 20.6 (C12), 22.8 (C1), 25.1 (C9), 26.9 (C8), 30.2 (C6), 40.0 (C7), 109.1 (C11), 132.1 (C4), 135.7 (C5), 148.7 (C10), 174.5 (C3), 178.1 (C2) ppm. $^{195}Pt$ NMR (107.51 MHz, DMSO-$d_6$): ¢ 1210 ppm. ESI-MS (positive ion mode): 525.3 *m/z*. Calc. for $[C_{12}H_{23}Cl_2N_2O_4Pt]^+$ 525.3 *m/z* $[M+H]^+$. Solubility in water (25 °C): 0.97±0.08 mM.

**Microwave assisted synthesis of complexes 1.** A solution in anhydrous acetone of acyl chloride of **PA** ($6.65\times10^{-4}$ mol, 5 eq) was added in a microwave vessel to a suspension of complex **i1** (0.05 g, $1.33\times10^{-4}$ mol, 1 eq) in anhydrous acetone to obtain a maximum volume of 5 mL. Excess pyridine (50 μL) was added dropwise to the stirring reaction mixture and the vessel was capped and introduced into the microwave cavity. The microwave unit was programmed to heat the vessel content to 55 °C over a 5-min ramp period and then hold at this temperature for 1 h; the power was automatically set at 50 W. During this time the mixture was stirred with a magnetic bar. After heating, the vessel was allowed to cool to room temperature before removing it from the cavity. The solution obtained was transferred in a round bottomed flask and dried under vacuum. The resulting oil was treated with hexane, diethyl ether and then water to yield a yellow powder. Yield: 0.048 g, 69%.

**Synthesis of complex 2.** The oily acyl chloride previously obtained ($3.74\times10^{-4}$ mol, 2.5 eq) was dissolved in anhydrous acetone (3 mL) and added to a suspension of 0.05 g ($1.50\times10^{-4}$ mol, 1 eq) of complex **i2** in anhydrous acetone (2 mL). Excess pyridine (50 μL) was added dropwise to the reaction mixture, which was then stirred, heated up to 70°C in a round bottomed flask equipped with a reflux condenser and left overnight. The yellow-orange suspension was dried under vacuum and the resulting oil was treated with hexane first and then water to yield a yellow powder. Yield: 0.051 g (54%). $^1H$ NMR (500.13 MHz, DMSO-$d_6$): ¢ 1.33–1.38 (m, 2H, H8), 1.72 (m, 6H, H12), 1.76–1.78 (m, 2H, H8'), 2.03 (m, 2H, H6), 2.06 (m, 2H, H7), 2.08 (m, 2H, H9), 2.24–2.27 (m, 2H, H6'), 2.32–2.36 (m, 2H, H9'), 4.71 (br. s, 1H, H11), 4.73 (br. s, 1H, H11'), 6.57 (m, 6H, N$H_3$), 6.70 (m, 2H, H5) ppm. $^{13}C$ NMR (125.76 MHz, DMSO-$d_6$): ¢ 20.6 (C12), 25.1 (C9), 26.9 (C8), 30.2 (C6), 40.0 (C7), 109.1 (C11), 132.1 (C4), 135.7 (C5), 148.7 (C10), 174.4 (C3) ppm. $^{195}Pt$ NMR (107.51 MHz, DMSO-$d_6$): ¢ 1194 ppm. ESI-MS (positive ion mode): 631.1 *m/z*. Calc. for $[C_{20}H_{33}Cl_2N_2O_4Pt]^+$ 631.5 *m/z* $[M+H]^+$. Solubility in water (25 °C): 0.027±0.007 mM.

**Microwave assisted synthesis of complex 2.** A solution in anhydrous acetone of acyl chloride of **PA** ($3.74\times10^{-4}$ mol, 2.5 eq) was added in a microwave vessel to a suspension of complex **i2** (0.05 g, $1.50\times10^{-4}$ mol, 1 eq) in anhydrous acetone to obtain a maximum volume of 5 mL. Excess pyridine (50 µL) was added dropwise to the stirring reaction mixture and the vessel was capped and introduced into the microwave cavity. The microwave unit was programmed to heat the vessel content to 55 °C over a 5-min ramp period and then hold at this temperature for 1 h; the power was automatically set at 50 W. During this time, the mixture was stirred with a magnetic bar. After heating, the vessel was allowed to cool to room temperature before removing it from the cavity. The solution obtained was transferred in a round bottomed flask and dried under vacuum. The resulting oil was treated with hexane and then water to yield a yellow powder. Yield: 0.045 g, 48%.

**Synthesis of $^{15}NH_3$-containing complexes 1 and 2.** The syntheses of complexes **1** and **2** containing $^{15}N$ ammonia were the same of those containing $^{14}NH_3$,[28, 86] but starting from *cis*-$[PtCl_2(^{15}NH_3)_2]$.[31, 87] The relevant characterization data are reported below. **$^{15}$N-1**. $^{15}N$ NMR (50.70 MHz, $H_2O$): ¢ -40.5 with satellite peaks at -37.9 ppm and -43.1 ppm ($^1J_{15N\text{-}195Pt}$ = 263.2 Hz, $^2J_{1H\text{-}195Pt}$ = 50.0 Hz) ppm. ESI-MS (positive ion mode): 527.2 *m/z* $[M+H]^+$. Calc. for $[C_{12}H_{23}Cl_2{}^{15}N_2O_4Pt]^+$ 527.1 *m/z* $[M+H]^+$. **$^{15}$N-2**. $^{15}N$ NMR (50.70 MHz, $H_2O$): ¢ -36.8 ppm. ESI-MS (positive ion mode): 633.4 *m/z* $[M+H]^+$. Calc. for $[C_{20}H_{33}Cl_2{}^{15}N_2O_4Pt]^+$ 633.1 *m/z* $[M+H]^+$.

**Lipophilicity and water solubility.** Chromatographic analysis was used to evaluate the capacity factors of the compounds as reported elsewhere.[38, 88, 89] Briefly, a chromatogram for each complex (0.5 mM) was run on a C18 column Phenosphere-NEXT (5-µm, 250×4.6 mm ID) with 15 mM formic acid/$CH_3OH$ 30/70 as mobile phase. The corresponding retention time tR was used to calculate log *k'* ($k' = (t_R - t_0) / t_0$); KCl was the internal reference to determine the column dead-time, $t_0$. The water solubility of the Pt(IV) complexes was determined preparing their saturated solutions in ultrapure water, which were stirred in the dark at 25 °C. After 24 h the solid residue was filtered off (0.20 µm cellulose filters) and the Pt content of the solutions was determined by means of ICP-MS (see below).

**Stability in solution and reduction with cytosol.** The solution behavior of the complexes was studied in two conditions: *i)* 2 mM HEPES buffer (HEPES = 4-(2-hydroxyethyl)-1-piperazineethanesulfonic acid, pH = 7.5) with $CH_3OH$ as a cosolvent (10% v/v for **1** and 30% v/v for **2**; final [Pt] was 0.5 mM for **1** and 0.1 mM for **2**); *ii)* cell culture medium RPMI 1640 with $CH_3OH$ as cosolvent (10% v/v for **1** and 20% v/v for **2**; final [Pt] was 0.1 mM for **1** and at saturation for **2**). For these experiments, the complexes were dissolved in methanol, then the organic solution was added to the buffer and the reaction followed for 72 h at 37 °C. The area of the chromatographic peaks of the Pt complexes was monitored in HPLC-MS. The mobile phase was a mixture of 15 mM aqueous HCOOH and $CH_3OH$ in a ratio depending on the experiment (see ESI for details).

For $^{15}N$-NMR measurements concerning reduction propensity, an aliquot (20 µl) of a saturated solution (< 150 mM) of **2** in DMF was diluted in cytosolic extract of A-549 cells (450 µl) and $D_2O$ (30 µL) was added at 25°C.The fresh cytosolic extract of about $2\times10^7$ A-549 cells was obtained with FractionPrep (first step only) following manufacturer's instructions.[51, 90]

**Biological evaluations**

**Antiproliferative activity.** The compounds under investigation were tested on ovarian endometrioid adenocarcinoma A2780 (ICLC HTL98008), embryonal carcinoma of the testis NTERA-2 clone D1 (also known as NT2/D1, ICLC HTL97025), lung adenocarcinoma A-549 (ICLC HTL03001), colon carcinoma HCT 116 (ECACC 91091005), HT-29 (ICLC HTL99026), and breast invasive ductal adenocarcinoma MCF-7 (ECACC 86012803). Moreover, four cell lines derived from pleural effusions of untreated malignant pleural mesothelioma (MPM) patients were used: BR95 (epithelioid phenotype) MG06 (biphasic, but predominantly epithelioid phenotype), MM98 (sarcomatoid phenotype) and its cisplatin-resistant subline MM98R derived from wild type by exposure to sub-lethal concentrations of cisplatin for several months were also used.[91-93] Additionally, primary human mesothelial cell line (HMC) was established with cells obtained by scraping the inner surface of the wall of the surgically removed hernial sacs.[91, 92] The non-MPM cells were purchased from European Collection of Cell Cultures (ECACC, UK) or Interlab Cell Line Collection (ICLC, Genova, Italy), whereas the MPM and HMC cell lines were obtained from the Hospital of Alessandria (Pathology Unit). The following media were used to culture the cells: RPMI 1640 (Thermo Fisher Scientific, Rodano, Italy) for A2780, NT2/D1 and A-549 cells; McCoy's 5A (Thermo Fisher Scientific, Rodano, Italy) for HCT 116 and HT-29 cells; Ham's F10 (GIBCO, Invitrogen Life Science, San Giuliano Milanese, Italy) for BR95, MG06 and HMC; Dulbecco's modified Eagle's medium (DMEM) (Thermo Fisher Scientific, Rodano, Italy) for MCF-7, MM98 and MM98R. All media contained L-glutamine (2 mM) and were supplemented with penicillin (100 IU mL-1), streptomycin (100 mg L-1) and 10% heat inactivated fetal bovine serum (FBS). Cell culture and treatment were carried out at 37 °C in a 5% CO2 humidified chamber. Cisplatin was dissolved in 0.9% w/v NaCl aqueous solution brought to pH 3 with HCl (final stock concentration 1 mM). Complexes 1 and 2 were dissolved in DMSO (final stock concentration 5 mM) and immediately used. These mother solutions were diluted in complete medium to the required concentration range and the total co-solvent concentration never exceeded 0.1% v/v. This concentration was found to be non-toxic to the cells tested (control). Moreover, the real Pt content in the culture medium after each serial dilution was checked by means of ICP-MS after filtration with a PTFE syringe filter (pore size 0.2 µm) to remove possible undissolved residues. Cells were treated with the compounds under investigation for 72 h. To assess the growth inhibition of the compounds, a cell viability test (*i.e.*, the resazurin reduction assay) was used. Briefly, $2\times10^3$ cells per well were seeded in black sterile tissue-culture treated 96-well plates. At the end of the treatment, viability was assayed by 100 µg mL-1 resazurin (Acros Chemicals, France) in fresh medium for 1 h at 37 °C, and the amount of the reduced product, resorufin, was measured

 

by means of fluorescence (excitation wavelength $^{a}\lambda_{exc}$ = 535 nm, emission wavelength $^{a}\lambda_{em}$ = 595 nm) with a Tecan Infinite F200Pro plate reader (Tecan, Austria). In each experiment, cells were challenged with the drug candidates at different concentrations and the final data were calculated from at least three replicates of the same experiment performed in triplicate. The fluorescence of 8 wells containing medium without cells were used as a blank. Fluorescence data were normalized to 100% cell viability for non-treated cells. Half-inhibiting concentration ($IC_{50}$), defined as the concentration of the drug reducing cell viability by 50%, was obtained from the dose-response sigmoid using Origin Pro (version 8, Microcal Software, Inc., Northampton, MA, USA).

**Clonogenic assay.** For the clonogenic assay, $1\times10^3$ A-549 or HCT 116 cells *per* well were seeded in complete medium in six-well plates. After 24 h the cells were washed with phosphate buffered saline (PBS) and treated with the compounds under investigation ($IC_{50}$ concentration for each cell line). After 72 h of treatment the drug-containing medium was removed and then cells were washed with PBS and incubated in drug-free medium for a week. Finally, the medium was removed, and the colonies were fixed and stained with a solution containing PBS, 1% v/v methanol, 1% v/v formaldehyde and 0.05% w/v Crystal Violet. After 20 min, the solution was removed, and each well was washed with ultrapure water. Finally, the visible colonies (more than 50 cells) in each plate (if any) can be counted for each treatment and the surviving fraction of cells can be calculated with respect to untreated samples.[94]

**Multicellular Tumor Spheroids (MCTS).** Spheroids from A-549 cells were obtained by using a previously reported microplate-based protocol.[56] Briefly, an initial seed in U-shaped, 96-well polypropylene plates of A-549 cells gave spheroids after 4 h. The spheroids (after medium removal by gentle aspiration) were challenged with drug-containing medium (200 µL *per* well) for 72 h, then drug-free medium was replaced twice a week until the experiment was stopped. At the same time points, pictures of at least three spheroids per each experiment were taken at 4× magnification and the dimensions of spheroids were assessed using the native Leica Application Suite software (version 2.0, Leica Microsystems).[95] The spheroid volume was calculated from the mean diameter and reported as fold change with respect to the time zero of the treatment.

**Combination index (CI).** In order to verify the synergy between **PA** and cisplatin, A-549 cells were treated with increasing concentrations of cisplatin or **PA**, and a mixture of them in a fixed 1:600 ratio, according to their respective $IC_{50}$ values and considering that **2** will produce two **PA** moieties after reduction. The experiment was repeated three times. According to the method of Chou and Talalay,[66, 96, 97] the interaction between cisplatin and **PA** was computed in terms of combination index (*CI*) for non-mutually exclusive drugs by using the following equation:

$$CI = \frac{C1_m}{C1_a} + \frac{C2_m}{C2_a} + \frac{C1_m C2_m}{C1_a C2_a},$$

where $C1$ and $C2$ are the drug concentrations used in the mix ($C1_m$ and $C2_m$) or alone ($C1_a$ and $C2_a$) to obtain the same level of residual viability. Based on the actual experimental data, the *CI* values were calculated by solving the equation over a wide range of residual viability (from 15 to 90%, obtained from the sigmoidal regression). These data were then used to generate residual viability *vs. CI* plots, which is an effect-oriented means of presenting synergism or antagonism. Interpretation of *CI* values is defined such that $CI = 1$ indicates an additive effect, and $CI < 1$ and a $CI > 1$ indicate synergism and antagonism, respectively.

**Cellular accumulation.** A-549 cells were seeded in 10 mm Petri dishes (for the 4 h and 4 h + 20 h recovery treatments) or 175 $cm^2$ flasks (for the 24 h treatment, see "DNA platination") and challenged with the complexes under investigations (10 µM) in complete medium. At the end of the exposure, cells were washed three times with phosphate buffered saline (PBS), detached from the Petri dishes using 0.05% Trypsin 1X + 2% EDTA (HyClone, Thermo Fisher) and harvested in fresh complete medium. An automatic cell counting device (Countess®, Life Technologies), was used to measure the number and the mean diameter from every cell count. For the cellular Pt accumulation analysis, the cells were transferred into a borosilicate glass tube and centrifuged at 1100 rpm for 5 min at room temperature. The supernatant was carefully removed by aspiration, while about 200 µL of the supernatant was left to limit the cellular loss. Cellular pellets were stored at −80 °C until mineralization. Platinum content determination was performed by ICP-MS (Thermo Optek X Series 2). Mineralization was performed by the addition of 70% w/w $HNO_3$ to each sample (after defrosting), followed by incubation for 1 h at 60 °C in an ultrasonic bath. Before the ICP-MS measurement, the $HNO_3$ was diluted to a final 1% concentration. The instrumental settings were optimized to yield maximum sensitivity for platinum, and the most abundant isotopes of Pt and In (used as internal standard) were quantified at *m/z* 195 and 115, respectively. The quantity of Pt found in cells after drug treatment and normalized upon the cell number (cellular Pt accumulation) was expressed as ng Pt per $10^6$ cells. At time zero of the treatment, 100 µL of medium was taken out from each sample to check the extracellular Pt concentration, $[Pt]_{EC.}$ The mean cellular volume, calculated from the actual mean cell diameter measured for every sample, was used to obtain the intracellular Pt concentration, $[Pt]_{IC}$. The ratio between the intra- and actual extra-cellular concentrations, is defined as accumulation ratio (AR):[98]

$$AR = \frac{[Pt]_{IC}}{[Pt]_{EC}}$$

Statistical significance was determined using one-way analysis of variance (ANOVA) with post-hoc Tukey's test with Origin Pro (version 8, Microcal Software, Inc., Northampton, MA, USA). Only $p$ values < 0.05 were considered statistically significant. Each analysis was carried out in triplicate.

**DNA platination.** A-549 cells were seeded in 175 $cm^2$ flasks and treated for 4 h, 4 h + 20 h recovery, and 24 h with the complexes under investigations (10 µM) as described above. From the same sample, about $5\times10^6$ cells were used for cellular accumulation analysis, whereas about $20\times10^6$ cells were used for the DNA platination analysis. For the DNA platination analysis, the cells were transferred into a plastics tube and

centrifuged at 1100 rpm for 5 min at room temperature. The supernatant was carefully removed by aspiration, and the cell pellets were stored at −20 °C until the total genomic DNA was extracted with a commercial kit (PerfectPure Cultured Mammalian Cells, 5Prime-Eppendorf), following the manufacturer's instructions. Briefly, during cell lysis, DNA was purified by RNAse A and proteinase K treatment, then extracted on silica-based centrifugation columns. After washing, DNA was eluted in 300 µL of elution buffer. An amount of 8 µL of sample or elution buffer (used as blank) was diluted in TE buffer (10 mM Tris–HCl, 1 mM EDTA, pH 8.0) to 80 µL, corresponding to a 0.5 cm path length in UV-transparent microplate half-area wells (UVStar®, Greiner Bio-one). Absorbance at 260 nm ($A_{260}$, relative to nucleic acids) and 280 nm ($A_{280}$, relative to proteins) was recorded from triplicate wells. For each well, $A_{260}$ and $A_{280}$ were corrected by subtraction of the background, then the purity of the samples was verified by means of the $A_{260}$ to $A_{280}$ ratio. After the subtraction of mean $A_{260}$ of blank wells, the DNA concentration was computed from the corrected $A_{260}$ by means of a calibration curve obtained with calf thymus DNA. Under these conditions an absorbance of 1 unit at 260 nm corresponds to 100 µg of DNA per mL. The remaining amount of DNA elution buffer was transferred into a borosilicate glass tube and its precise volume determined by weight to compute the total amount of DNA, then stored at −20 °C until mineralization. The amount of Pt bound to DNA was expressed as pg of Pt per µg of DNA experimentally found. Statistical significance was determined using one-way analysis of variance (ANOVA) with post-hoc Tukey's test with Origin Pro (version 8, Microcal Software, Inc., Northampton, MA, USA). Only $p$ values < 0.05 were considered statistically significant. Each analysis was carried out in triplicate.

**Caspase 3 activity.** A-549 cells ($1\times10^5$) were seeded in 96-well black tissue culture (TC) plates the day before treatment, that was performed with increasing concentrations of the Pt compounds and **PA**. After 24 h, the cells were washed by *Earle's Balanced Salt Solution (EBSS)* and lysed on ice with 25 µM lysis buffer (10 mM HEPES, 2 mM EDTA, 2 mM DTT, 0.1% CHAPS, pH 7.4). Then, 200 µL the caspase-3 fluorescent substrate, Ac-DEVD-AFC (*N*-Acetyl-Asp-Glu-Val-Asp-7-amino-4-trifluoromethylcoumarin, 0.01 g $L^{-1}$ in lysis buffer), was added to all wells, mixed, and 200 µL of each sample were transferred to a black microtiter plate. The activity was followed for 1 h, by means of fluorescence at $^{a}_{exc}$ = 390 nm, $^{a}_{em}$ = 520 nm, normalized over the blank.[99] Final fold activity was computed with respect to control wells and normalized on the residual viability. The test was repeated in the presence of the caspase 3/7 inhibitor Ac-DEVD-CHO (N-Acetyl-Asp-Glu-Val-Asp-CHO) at 0.01 g $L^{-1}$ concentration.

**Mitochondrial transmembrane potential assay.** The mitochondrial transmembrane potential ($\Delta v_M$) was assayed in black-walled, clear bottom, tissue culture treated, sterile 96 wells plates (ViewPlate 96 F, Perkin-Elmer, Milan) by means of the mitochondria staining kit (Sigma-Aldrich, Milan), following manufacturer's instructions. The fluorescence of the JC-1 dye (5,5′,6,6′-tetrachloro-1,1′,3,3′-tetraethylbenzimidazolocarbocyanine iodide) was recorded at $^{a}_{exc}$ = 525 nm, $^{a}_{em}$ = 590 nm for red fluorescent JC-1 aggregates (formed since the dye concentrates in the mitochondrial matrix, due to the electrochemical potential gradient) and at $^{a}_{exc}$ = 490 nm, $^{a}_{em}$ = 530 nm for green fluorescent JC-1 monomers (since the dissipation of the mitochondrial membrane potential leads to the dye dispersion throughout the entire cell). Valinomycin was used as positive control. Statistical significance was determined using one-way analysis of variance (ANOVA) with post-hoc Tukey's test with Origin Pro (version 8, Microcal Software, Inc., Northampton, MA, USA). Only $p$ values < 0.05 were considered statistically significant. Each analysis was carried out in triplicate.

**ROS assay.** The 2′,7′-dichlorofluorescein diacetate ($H_2$DCF-DA) dye was used to detect reactive oxygen species (ROS) levels. A-549 cells ($2\times10^5$) were seeded in black sterile 96-well TC plates the day before treatment (8 wells *per* treatment), that was performed with cisplatin (50 µM), **PA** (1 mM) and **2** (1 µM). After 24 h, 3 wells of each treatment were used to assess residual viability by means of the resazurin reduction assay, while the remaining wells were loaded with 10 µM $H_2$DCF-DA in EBSS at 37 °C for 30 min, in the dark. Immediately before the end of loading $H_2O_2$ 5 mM (final concentration) was added as positive control, while a control column received 10 mM *N*-acetylcysteine (NAC), a well-known antioxidant, as negative control of each condition. After 2 washes by EBSS, oxidized DCF fluorescence was measured at $^{a}_{exc}$ = 485 nm and $^{a}_{em}$ = 535 nm. Data were normalized on viability. Statistical significance was determined using one-way analysis of variance (ANOVA) with post-hoc Tukey's test with Origin Pro (version 8, Microcal Software, Inc., Northampton, MA, USA). Only $p$ values < 0.05 were considered statistically significant. Each analysis was carried out in triplicate.

**Quantitative Reverse Transcription PCR (RT-qPCR).** A-549 cells ($2\times10^6$) were seeded on T25 flasks and allowed to attach for 24 h. The treatment was performed with equitoxic concentrations (*i.e.*, 50 µM cisplatin, 1 mM **PA** and 1 µM **2**). After 24 h, RNA was extracted and purified by DNAse treatment with a commercial kit (RNASPIN MINI, GE Healthcare); then it was quantified and checked for purity by means of absorbance at λ = 260, 280, and 340 nm in UV-Star half area UV transparent plate (Brand) with the above-mentioned microplate reader. For each sample, 1 µg of RNA was retrotranscribed (RT) to cDNA with the Revertaid cDNA First strand kit (Thermo-Fisher) using random hexamer primers at 45 °C, following the manufacturer's instructions. qPCR was performed in triplicate on each sample (10 ng) to detect the expression levels of the genes under investigation and the reference genes. Primer sequences were designed using the NCBI tool and checked for target specificity including splice variants (see ESI, Table S1). Reactions were based on the SsoFast EvaGreen Supermix (Bio-Rad) in the presence of 0.4 µM primer pairs except for RNA18S (0.2 µM), according to the manufacturer's instructions, in a reaction volume of 10 µL. In order to compute reaction efficiency, a standard curve was performed for each master mix. qPCR was performed using the CFX368 thermal cycler (Bio-Rad). The reaction conditions were: 95 °C for 1 min, followed by 45 cycles at 98 °C for 5 s and anneal–extend step for 5 s at 60 °C, with data

 

collection. At the end of these cycles, a melting curve (65 °C to 95 °C, with plate read every 0.5 °C) was performed to assess the specificity of the amplification product by single peak melting temperature verification. Results were normalized on the reference genes and on the control according to the ΔΔCq method. All data analyses were performed with the built-in software (CFX Manager, Bio-Rad).

**Migration and invasion assays.** The migration and invasion ability of A-549 cells was evaluated using 6.5 mm Corning® Transwell® (Life Sciences) with 8.0 µm Pore PET Membrane Insert.[100] In particular, for the migration assay 600 µL *per* chamber of complete medium (except in the negative control with 600 µL of FBS-free medium) were inserted into the receiving wells (lower chambers of Transwell®). The plate containing the Transwell® was incubated for 1 h at 37 °C and 5% $CO_2$. The cells were starved in a medium supplemented with 0.5% FBS, penicillin 100 IU $mL^{-1}$ and streptomycin (100 mg $L^{-1}$) for 24 h to induce them to migrate towards nutrients. The cells were then detached using 0,05% Trypsin 1X + 2% EDTA, diluted in medium without serum, and centrifuged at 1100 rpm for 5 min. The cells were resuspended in fresh complete medium containing 0.1% w/v BSA (Bovine Serum Albumin) at a concentration of $4\times10^6$ cells $mL^{-1}$. This suspension (150 µL *per* chamber) was added in the upper chamber (insert) of each Transwell® and challenged with serum-free medium (150 µL *per* chamber), with or without the tested compound, in the corresponding lower chamber. The final concentrations of the compounds were 50 µM for cisplatin, 1 mM for **PA**, and 1 µM for **2**. The wells were incubated at 37 °C and 5% $CO_2$ for 24 h. Migratory cells, able to extend protrusions towards chemo-attractants, passed through the pores of the membrane. The medium was then removed from the upper and lower chambers of each Transwell® and the cells that migrated across the membrane surface were fixed and stained for 15 min with 600 µL *per* chamber of a solution of methanol and crystal violet (see 4.2.3. Clonogenic assay). After removal of excess dye, non-migrated cells remained at the upper surface of the membranes were carefully removed with cotton swabs. Pictures of the stained membranes were taken using an inverted microscope (Leica® DM IL LED) with the native Leica Application Suite software (version 2.0, Leica Microsystems). For the invasion assay, 100 µL of a solution (Tris HCl 0.01 M, 0.7% NaCl, pH 8) containing 300 µg $mL^{-1}$ of extracellular matrix (Corning® Matrigel® Basement Membrane Matrix) were added to the surface of the membrane of each Transwell® insert at 4 °C. After 2 h incubation at 37 °C excess liquid was removed avoiding to completely dry the gel. The experiment was then carried out as described above for the migration assay.

**Wound healing assay.** For the wound healing assay, A-549 cells were seeded on glass slides (22 mm × 22 mm) located in 6-well plates. After 24 h, having obtained 90% confluence, a disposable pipette tip (volume of 1 mL) was used to scratch the wounds on the midline of the coverslip, then the scratch was immediately measured (time point 0 h). After this procedure, A-549 were treated with **CDDP** at 50 µm, **2** at 1 µm and **PA** 1 mM respectively. After 24 h, three measurements were made relating to the closure of the wound. All data were reported as the percentage of mean value ± standard deviation (sd) of wound closure (time point 24 h). Statistical significance was determined using one-way analysis of variance (ANOVA) with post-hoc Tukey's test with Prism 5 (GraphPad Software, San Diego, CA, USA). Only $p$ values < 0.05 were considered statistically significant. Each analysis was carried out in triplicate.

**Immunocytochemical reactions: fluorescence microscopy evaluation.** After wound healing assay analysis, the coverslips were fixed with 4% formalin for 20 min and post-fixed with 70% ethanol at -20°C for at least 24 h. Samples were rehydrated for 10 min in PBS and then immunolabeled with primary antibody for Active-Cdc42 (1:100, monoclonal mouse anti-active-Cdc42 BIOMOL GmbH, Hamburg, Germany) for 1 h at room temperature in a dark moist chamber. After some washes in PBS, coverslips were incubated with the secondary antibody (1:200 in PBS, Alexa Fluor 594, Molecular Probes) for 45 min. After that, sections were counterstained for DNA with 0.1 µg mL-1 Hoechst 33258 (Sigma-Aldrich, Milano, Italy), washed with PBS, and mounted in a drop of Mowiol (Calbiochem, Inalco, Italy), for fluorescence microscopy analysis. An Olympus BX51 microscope equipped with a 100-W mercury lamp was used under the following conditions: 330–385 nm excitation filter (excf), 400 nm dichroic mirror (dm) and 420 nm barrier filter (bf) for Hoechst 33258; 540 nm excf, 580 nm dm and 620 nm bf for Alexa 594. Images were recorded with an Olympus MagniFire camera system and processed with the Olympus Cell F software. To quantify fluorescence intensity of protein expression, the optical density (OD), was measured using ImageJ Software. The statistical analysis was carried out by calculating the OD average per cell in control and each treatment conditions. Then values were expressed as the mean ± sd and differences were compared using one-way analysis of variance (ANOVA) with post-hoc Tukey's test with Prism 5 (GraphPad Software, Version 5.03, San Diego, CA, USA). Only $p$ values < 0.05 were considered statistically significant.

## Conclusions

The multi-action Pt(IV) prodrugs may offer the chance to associate the cytotoxic activity of cisplatin with the synergistic and/or adjuvant activity of bioactive ligands coordinated in axial position. The *combo* **2** represents a successful application of such a strategy. Actually:

1. a moderate synergistic antiproliferative activity between free cisplatin and **PA** (*i.e.*, the metabolites simultaneously released by **2** after the intracellular Pt(IV) → Pt(II) reduction) has been demonstrated.
2. an additional feature of **2** was observed at the level of the migration process of A-549 lung adenocarcinoma cells. The results obtained show that **2** induces both a reduction in the migrant population and a reduction in the markers related to this process.

In the *combo*, the released cisplatin moiety exerts mainly the cytotoxic effect, whereas the **PA** ligand is responsible for the antimetastatic activity. These effects are obviously showed by the free molecules, but at much higher concentrations with

respect to **2**. The synergistic cellular accumulation of (highly lipophilic) **2** is the main reason for the good performance of this prodrug with respect to those of the (less lipophilic) separate components.

In conclusion, **2** may be considered a "true" multi-action molecule exhibiting both cytotoxic and antimetastatic activity.

## Conflicts of interest

There are no conflicts to declare.

## Acknowledgements

This research is original and has a financial support of the Università del Piemonte Orientale (UPO). Moreover, it has been carried out within the HERMES project, "*Progetto finanziato attraverso l'offerta di indennizzo ai residenti di Casale Monferrato deceduti o affetti da mesotelioma*" (Project funded by offer of compensation to the residents of Casale Monferrato died or suffering from mesothelioma). We are indebted to Inter-University Consortium for Research on the Chemistry of Metals in Biological Systems (CIRCMSB, Bari, Italy), for providing opportunities of stimulating discussion during the annual meetings. Finally, we thank Prof. G. Sava and Prof. A. Bergamo (University of Trieste, Italy) for their precious advice.

## Notes and references

1. A. Bergamo and G. Sava, *Chemical Society Reviews*, 2015, **44**, 8818-8835.
2. A. Bergamo, P. J. Dyson and G. Sava, *Coordination Chemistry Reviews*, 2018, **360**, 17-33.
3. S. M. Meier-Menches, C. Gerner, W. Berger, C. G. Hartinger and B. K. Keppler, *Chemical Society Reviews*, 2018, **47**, 909-928.
4. F. P. Intini, J. Zajac, V. Novohradsky, T. Saltarella, C. Pacifico, V. Brabec, G. Natile and J. Kasparkova, *Inorganic Chemistry*, 2017, **56**, 1483-1497.
5. S. A. Perez, C. de Haro, C. Vicente, A. Donaire, A. Zamora, J. Zajac, H. Kostrhunova, V. Brabec, D. Bautista and J. Ruiz, *Acs Chemical Biology*, 2017, **12**, 1524-1537.
6. J. Pracharova, V. Novohradsky, H. Kostrhunova, P. Starha, Z. Travnicek, J. Kasparkova and V. Brabec, *Dalton Transactions*, 2018, **47**, 12197-12208.
7. H. L. Song, N. J. Rogers, S. J. Allison, V. Brabec, H. Bridgewater, H. Kostrhunova, L. Markova, R. M. Phillips, E. C. Pinder, S. L. Shepherd, L. S. Young, J. Zajac and P. Scott, *Chemical Science*, 2019, **10**, 8547-8557.
8. L. L. Ma, X. D. Lin, C. Li, Z. F. Xu, C. Y. Chan, M. K. Tse, P. Shi and G. Y. Zhu, *Inorganic Chemistry*, 2018, **57**, 2917-2924.
9. E. Gabano, M. Ravera and D. Osella, *Dalton Transactions*, 2014, **43**, 9813-9820.
10. D. Gibson, *Dalton Transactions*, 2016, **45**, 12983-12991.
11. R. G. Kenny, S. W. Chuah, A. Crawford and C. J. Marmion, *European Journal of Inorganic Chemistry*, 2017, 1596-1612.
12. H. H. S. Chow, D. Salazar and I. A. Hakim, *Cancer Epidemiology Biomarkers & Prevention*, 2002, **11**, 1472-1476.
13. T. C. Chen, C. O. Da Fonseca and A. H. Schonthal, *American Journal of Cancer Research*, 2015, **5**, 1580-1593.
14. S. Bardon, K. Picard and P. Martel, *Nutrition and Cancer-an International Journal*, 1998, **32**, 1-7.
15. S. Bardon, V. Foussard, S. Fournel and A. Loubat, *Cancer Letters*, 2002, **181**, 187-194.
16. M. H. Gelb, F. Tamanoi, K. Yokoyama, F. Ghomashchi, K. Esson and M. N. Gould, *Cancer Letters*, 1995, **91**, 169-175.
17. Y. Pylayeva-Gupta, E. Grabocka and D. Bar-Sagi, *Nature Reviews Cancer*, 2011, **11**, 761-774.
18. N. Berndt, A. D. Hamilton and S. M. Sebti, *Nature Reviews Cancer*, 2011, **11**, 775-791.
19. H. van Hattum and H. Waldmann, *Chemistry & Biology*, 2014, **21**, 1185-1195.
20. A. D. Cox, C. J. Der and M. R. Philips, *Clinical Cancer Research*, 2015, **21**, 1819-1827.
21. X. D. Zhao and S. Subramanian, *Pharmacology & Therapeutics*, 2018, **181**, 76-84.
22. T. J. Raphael and G. Kuttan, *Journal of Experimental & Clinical Cancer Research*, 2003, **22**, 419-424.
23. T. J. Raphael and G. Kuttan, *Immunopharmacology and Immunotoxicology*, 2003, **25**, 285-294.
24. D. Samaila, B. J. Toy, R. C. Wang and J. A. Elegbede, *Anticancer Research*, 2004, **24**, 3089-3095.
25. L. Yeruva, K. J. Pierre, A. Elegbede, R. C. Wang and S. W. Carper, *Cancer Letters*, 2007, **257**, 216-226.
26. S. C. Dhara, *Indian Journal of Chemistry*, 1970, **8**, 193-194.
27. F. D. Rochon and L. M. Gruia, *Inorganica Chimica Acta*, 2000, **306**, 193-204.
28. J. Z. Zhang, P. Bonnitcha, E. Wexselblatt, A. V. Klein, Y. Najajreh, D. Gibson and T. W. Hambley, *Chemistry-a European Journal*, 2013, **19**, 1672-1676.
29. M. Ravera, E. Gabano, I. Zanellato, F. Fregonese, G. Pelosi, J. A. Platts and D. Osella, *Dalton Transactions*, 2016, **45**, 5300-5309.
30. S. Shamsuddin, C. C. Santillan, J. L. Stark, K. H. Whitmire, Z. H. Siddik and A. R. Khokhar, *Journal of Inorganic Biochemistry*, 1998, **71**, 29-35.
31. M. S. Davies, M. D. Hall, S. J. Berners-Price and T. W. Hambley, *Inorganic Chemistry*, 2008, **47**, 7673-7680.
32. P. S. Pregosin, *Coordination Chemistry Reviews*, 1982, **44**, 247-291.
33. T. G. Appleton, J. R. Hall and S. F. Ralph, *Inorganic Chemistry*, 1985, **24**, 673-677.
34. E. Gabano, E. Marengo, M. Bobba, E. Robotti, C. Cassino, M. Botta and D. Osella, *Coordination Chemistry Reviews*, 2006, **250**, 2158-2174.
35. L. Ronconi and P. J. Sadler, *Coordination Chemistry Reviews*, 2008, **252**, 2239-2277.
36. S. J. Berners-Price, L. Ronconi and P. J. Sadler, *Progress in Nuclear Magnetic Resonance Spectroscopy*, 2006, **49**, 65-98.
37. P. Gramatica, E. Papa, M. Luini, E. Monti, M. B. Gariboldi, M. Ravera, E. Gabano, L. Gaviglio and D. Osella, *Journal of Biological Inorganic Chemistry*, 2010, **15**, 1157-1169.
38. G. Ermondi, G. Caron, M. Ravera, E. Gabano, S. Bianco, J. A. Platts and D. Osella, *Dalton Transactions*, 2013, **42**, 3482-3489.
39. A. C. Tsipis and I. N. Karapetsas, *Dalton Transactions*, 2014, **43**, 5409-5426.
40. W. J. Lambert, *Journal of Chromatography A*, 1993, **656**, 469-484.

 

41. S. Martel, D. Guillarme, Y. Henchoz, A. Galland, J.-L. Veuthey, S. Rudaz and P.-A. Carrupt, in *Molecular Drug Properties - Measurement and Prediction*, ed. R. Mannhold, Wiley-VCH, Weinheim, Germany, 2007, pp. 331-355.
42. E. Gabano, M. Ravera, F. Trivero, S. Tinello, A. Gallina, I. Zanellato, M. B. Gariboldi, E. Monti and D. Osella, *Dalton Transactions*, 2018, **47**, 8268-8282.
43. E. Gabano, M. Ravera, I. Zanellato, S. Tinello, A. Gallina, B. Rangone, V. Gandin, C. Marzano, M. G. Bottone and D. Osella, *Dalton Transactions*, 2017, **46**, 14174-14185.
44. M. Ravera, E. Gabano, I. Zanellato, A. Gallina, E. Perin, A. Arrais, S. Cantamessa and D. Osella, *Dalton Transactions*, 2017, **46**, 1559-1566.
45. I. V. Tetko, H. P. Varbanov, M. Galanski, M. Talmaciu, J. A. Platts, M. Ravera and E. Gabano, *Journal of Inorganic Biochemistry*, 2016, **156**, 1-13.
46. I. V. Tetko, I. Jaroszewicz, J. A. Platts and J. Kuduk-Jaworska, *Journal of Inorganic Biochemistry*, 2008, **102**, 1424-1437.
47. A. Kastner, I. Poetsch, J. Mayr, J. V. Burda, A. Roller, P. Heffeter, B. K. Keppler and C. R. Kowol, *Angewandte Chemie International Edition*, 2019, **58**, 7464-7469.
48. E. Wexselblatt, R. Raveendran, S. Salameh, A. Friedman-Ezra, E. Yavin and D. Gibson, *Chemistry-a European Journal*, 2015, **21**, 3108-3114.
49. E. Wexselblatt, E. Yavin and D. Gibson, *Angewandte Chemie-International Edition*, 2013, **52**, 6059-6062.
50. E. Wexselblatt and D. Gibson, *Journal of Inorganic Biochemistry*, 2012, **117**, 220-229.
51. A. Nemirovski, Y. Kasherman, Y. Tzaraf and D. Gibson, *Journal of Medicinal Chemistry*, 2007, **50**, 5554-5556.
52. M. Lopez-Lazaro, *Current Medicinal Chemistry*, 2015, **22**, 1324-1334.
53. M. Ravera, E. Gabano, I. Zanellato, I. Bonarrigo, E. Escribano, V. Moreno, M. Font-Bardia, T. Calvet and D. Osella, *Dalton Transactions*, 2012, **41**, 3313-3320.
54. I. Zanellato, I. Bonarrigo, E. Gabano, M. Ravera, N. Margiotta, P.-G. Betta and D. Osella, *Inorganica Chimica Acta*, 2012, **393**, 64-74.
55. M. Alessio, I. Zanellato, I. Bonarrigo, E. Gabano, M. Ravera and D. Osella, *Journal of Inorganic Biochemistry*, 2013, **129**, 52-57.
56. I. Zanellato, I. Bonarrigo, D. Colangelo, E. Gabano, M. Ravera, M. Alessio and D. Osella, *Journal of Inorganic Biochemistry*, 2014, **140**, 219-227.
57. D. J. Giard, S. A. Aaronson, G. J. Todaro, P. Arnstein, J. H. Kersey, H. Dosik and W. P. Parks, *JNCI: Journal of the National Cancer Institute*, 1973, **51**, 1417-1423.
58. O. Menyhart, H. Harami-Papp, S. Sukumar, R. Schafer, L. Magnani, O. de Barrios and B. Gyorffy, *Biochimica Et Biophysica Acta-Reviews on Cancer*, 2016, **1866**, 300-319.
59. H. R. Mellor, S. Snelling, M. D. Hall, S. Modok, M. Jaffar, T. W. Hambley and R. Callaghan, *Biochemical Pharmacology*, 2005, **70**, 1137-1146.
60. N. S. Bryce, J. Z. Zhang, R. M. Whan, N. Yamamoto and T. W. Hambley, *Chemical Communications*, 2009, 2673-2675.
61. J. Z. Zhang, N. S. Bryce, A. Lanzirotti, C. K. J. Chen, D. Paterson, M. D. de Jonge, D. L. Howard and T. W. Hambley, *Metallomics*, 2012, **4**, 1209-1217.
62. C. R. Thoma, M. Zimmermann, I. Agarkova, J. M. Kelm and W. Krek, *Advanced Drug Delivery Reviews*, 2014, **69**, 29-41.
63. M. Zanoni, F. Piccinini, C. Arienti, A. Zamagni, S. Santi, R. Polico, A. Bevilacqua and A. Tesei, *Scientific Reports*, 2016, **6**, 19103.
64. C. Berrouet, N. Dorilas, K. A. Rejniak and N. Tuncer, *Bulletin of Mathematical Biology*, 2020, **82**, 68.
65. T. C. Chou and P. Talalay, *European Journal of Biochemistry*, 1981, **115**, 207-216.
66. T. C. Chou and P. Talalay, *Advances in Enzyme Regulation*, 1984, **22**, 27-55.
67. M. Ravera, E. Gabano, I. Zanellato, I. Bonarrigo, M. Alessio, F. Arnesano, A. Galliani, G. Natile and D. Osella, *Journal of Inorganic Biochemistry*, 2015, **150**, 1-8.
68. Z. H. Siddik, *Oncogene*, 2003, **22**, 7265-7279.
69. R. Singh, A. Letai and K. Sarosiek, *Nature Reviews Molecular Cell Biology*, 2019, **20**, 175-193.
70. T. Abbas and A. Dutta, *Nature Reviews Cancer*, 2009, **9**, 400-414.
71. M. Agrawal and M. Gadgil, *Computers in Biology and Medicine*, 2012, **42**, 1141-1149.
72. L. G. T. Morris and T. A. Chan, *Cancer*, 2015, **121**, 1357-1368.
73. B. J. Aubrey, A. Strasser and G. L. Kelly, *Cold Spring Harbor Perspectives in Medicine*, 2016, **6**, 16.
74. U. Jungwirth, C. R. Kowol, B. K. Keppler, C. G. Hartinger, W. Berger and P. Heffeter, *Antioxidants & Redox Signaling*, 2011, **15**, 1085-1127.
75. D. S. Kalinowski, C. Stefani, S. Toyokuni, T. Ganz, G. J. Anderson, N. V. Subramaniam, D. Trinder, J. K. Olynyk, A. Chua, P. J. Jansson, S. Sahni, D. J. R. Lane, A. M. Merlot, Z. Kovacevic, M. L. H. Huang, C. S. Lee and D. R. Richardson, *Biochimica Et Biophysica Acta-Molecular Cell Research*, 2016, **1863**, 727-748.
76. P. Y. Zhang and P. J. Sadler, *European Journal of Inorganic Chemistry*, 2017, 1541-1548.
77. M. Ravera, E. Gabano, M. J. McGlinchey and D. Osella, *Inorganica Chimica Acta*, 2019, **492**, 32-47.
78. J. Marshall, in *Cell Migration: Developmental Methods and Protocols*, eds. C. M. Wells and M. Parsons, Humana Press, Totowa, NJ, 2011, pp. 97-110.
79. G. Benton, I. Arnaoutova, J. George, H. K. Kleinman and J. Koblinski, *Advanced Drug Delivery Reviews*, 2014, **79-80**, 3-18.
80. C. C. Liang, A. Y. Park and J. L. Guan, *Nature Protocols*, 2007, **2**, 329-333.
81. H. F. Liu, J. Ma, Y. G. Li, K. X. Yue, L. R. Li, Z. Q. Xi, X. Zhang, J. N. Liu, K. Feng, Q. Ma, S. T. Liu, S. D. Guo, P. G. Wang, C. J. Wang and S. Q. Xie, *Journal of Medicinal Chemistry*, 2019, **62**, 11324-11334.
82. Z. K. Liu, M. Wang, H. S. Wang, L. Fang and S. H. Gou, *European Journal of Medicinal Chemistry*, 2020, **194**.
83. C. Hoege, B. Pfander, G. L. Moldovan, G. Pyrowolakis and S. Jentsch, *Nature*, 2002, **419**, 135-141.
84. M. D. Maldonado and S. Dharmawardhane, *Cancer Research*, 2018, **78**, 3101-3111.
85. D. Ratto, B. Ferrari, E. Roda, F. Brandalise, S. Siciliani, F. De Luca, E. C. Priori, C. Di Iorio, F. Cobelli, P. Veneroni, M. G. Bottone and P. Rossi, *Cellular and Molecular Neurobiology*, 2020, **40**, 813-828.
86. G. Pelosi, M. Ravera, E. Gabano, F. Fregonese and D. Osella, *Chemical Communications*, 2015, **51**, 8051-8053.
87. M. S. Davies, M. D. Hall, S. J. Berners-Price and T. W. Hambley, *Inorganic Chemistry*, 2008, **47**, 7673-7680.

88. J. A. Platts, G. Ermondi, G. Caron, M. Ravera, E. Gabano, L. Gaviglio, G. Pelosi and D. Osella, *Journal of Biological Inorganic Chemistry*, 2011, **16**, 361-372.
89. J. A. Platts, S. P. Oldfield, M. M. Reif, A. Palmucci, E. Gabano and D. Osella, *Journal of Inorganic Biochemistry*, 2006, **100**, 1199-1207.
90. A. Nemirovski, I. Vinograd, K. Takrouri, A. Mijovilovich, A. Rompel and D. Gibson, *Chemical Communications*, 2010, **46**, 1842-1844.
91. E. Aldieri, C. Riganti, F. Silvagno, S. Orecchia, P. G. Betta, S. Doublier, E. Gazzano, M. Polimeni, A. Bosia and D. Ghigo, *American Journal of Respiratory Cell and Molecular Biology*, 2011, **45**, 625-631.
92. S. Orecchia, F. Schillaci, M. Salvio, R. Libener and P. G. Betta, *Lung Cancer*, 2004, **45**, S37-S43.
93. I. Zanellato, C. D. Boidi, G. Lingua, P. G. Betta, S. Orecchia, E. Monti and D. Osella, *Cancer Chemotherapy and Pharmacology*, 2011, **67**, 265-273.
94. N. A. P. Franken, H. M. Rodermond, J. Stap, J. Haveman and C. van Bree, *Nature Protocols*, 2006, **1**, 2315-2319.
95. L. Kamentsky, T. R. Jones, A. Fraser, M. A. Bray, D. J. Logan, K. L. Madden, V. Ljosa, C. Rueden, K. W. Eliceiri and A. E. Carpenter, *Bioinformatics*, 2011, **27**, 1179-1180.
96. T.-C. Chou, *Pharmacological Reviews*, 2006, **58**, 621-681.
97. T. C. Chou, *Cancer Research*, 2010, **70**, 440-446.
98. A. Ghezzi, M. Aceto, C. Cassino, E. Gabano and D. Osella, *Journal of Inorganic Biochemistry*, 2004, **98**, 73-78.
99. K. Kuželová, D. Grebeňová and B. Brodská, *Journal of Cellular Biochemistry*, 2011, **112**, 3334-3342.
100. R. Limame, A. Wouters, B. Pauwels, E. Fransen, M. Peeters, F. Lardon, O. De Wever and P. Pauwels, *Plos One*, 2012, **7**, e46536.